Journal of
Plankton Research

academic.oup.com/plankt

J. Plankton Res. (2021) 1–20. doi:10.1093/plankt/fbab006

BLOOFINZ - Gulf of Mexico

Phytoplankton community composition and biomass in the oligotrophic Gulf of Mexico

KAREN E. SELPH[1,*], RASMUS SWALETHORP[2], MICHAEL R. STUKEL[3], THOMAS B. KELLY[3], ANGELA N. KNAPP[3], KELSEY FLEMING[2], TABITHA HERNANDEZ[2] AND MICHAEL R. LANDRY[2]

[1]DEPARTMENT OF OCEANOGRAPHY, UNIVERSITY OF HAWAII AT MANOA, 1000 POPE ROAD, HONOLULU, HI 96822, USA, [2]SCRIPPS INSTITUTION OF OCEANOGRAPHY, 9500 GILMAN DRIVE, LA JOLLA, CA 92093-0227, USA AND [3]DEPARTMENT OF EARTH, OCEAN AND ATMOSPHERIC SCIENCE, FLORIDA STATE UNIVERSITY, TALLAHASSEE, FL 32306, USA

*CORRESPONDING AUTHOR: selph@hawaii.edu

Received October 13, 2020; editorial decision January 10, 2021; accepted January 10, 2021

Corresponding editor: Lisa Campbell

Biomass and composition of the phytoplankton community were investigated in the deep-water Gulf of Mexico (GoM) at the edges of Loop Current anticyclonic eddies during May 2017 and May 2018. Using flow cytometry, high-performance liquid chromatography pigments and microscopy, we found euphotic zone integrated chlorophyll a of ~10 mg m^{-2} and autotrophic carbon ranging from 463 to 1268 mg m^{-2}, dominated by picoplankton (<2 μm cells). Phytoplankton assemblages were similar to the mean composition at the Bermuda Atlantic Time-series Study site, but differed from the Hawaii Ocean Times-series site. GoM phytoplankton biomass was ~2-fold higher at the deep chlorophyll maximum (DCM) relative to the mixed layer (ML). *Prochlorococcus* and prymnesiophytes were the dominant taxa throughout the euphotic zone; however, other eukaryotic taxa had significant biomass in the DCM. Shallower DCMs were correlated with more prymnesiophytes and prasinophytes (Type 3) and reduced *Prochlorococcus*. These trends in ML and DCM taxonomic composition likely reflect relative nutrient supply—with ML populations relying on remineralized ammonium as a nitrogen source, and the taxonomically diverse DCM populations using more nitrate. These spatially separated phytoplankton communities represent different pathways for primary production, with a dominance of picoplankton in the ML and more nano- and microplankton at the DCM.

KEYWORDS: phytoplankton; Gulf of Mexico; oligotrophic; *Prochlorococcus*; prymnesiophytes

available online at academic.oup.com/plankt

INTRODUCTION

Phytoplankton community structure directly impacts upper trophic level organisms and export processes, and hence ecosystem function (Finkel *et al.*, 2010; Marañón, 2019; Michaels and Silver, 1988; Mouw *et al.*, 2016). While phytoplankton communities are well studied in coastal and shelf areas of the northern Gulf of Mexico (GoM), especially in areas influenced by the Mississippi River Outflow and plume (Chakraborty and Lohrenz, 2015; Jochem, 2003; Liu *et al.*, 2004; Qian *et al.*, 2003; Wawrik and Paul, 2004), most studies beyond the shelf break have been based on satellite observations (Hidalgo-González *et al.*, 2005; Lindo-Atichati *et al.*, 2012; Müller-Karger *et al.*, 1991; Teo *et al.*, 2007). The few exceptions included data from stations on the continental shelf/slope edge (Chakraborty and Lohrenz, 2015; Qian *et al.*, 2003) or used methods that gave an incomplete picture of composition and biomass of the community of the deep euphotic zone (Easson and Lopez, 2019; Williams *et al.*, 2015). Since the oceanic GoM habitat is important for commercially important and endangered fish species, filling this knowledge gap is essential for informed ecosystem-based management.

Oligotrophic regions like the northern and central GoM are typically dominated by cyanobacteria and picoeukaryotes, i.e. cells ≤ 2 μm in diameter, (Agawin *et al.*, 2000; Buitenhuis *et al.*, 2012; Goericke, 1998; Pasulka *et al.*, 2013), implying inefficient food webs (Buitenhuis *et al.*, 2012; Flombaum *et al.*, 2020). However, the substantial mesoscale variability within the GoM could lead to other food-web characteristics. One important impact on GoM productivity is the Loop Current (Biggs and Ressler, 2001), which is formed as the Caribbean Current and sheds westward-propagating mesoscale eddies as it moves northward from the Yucatan Channel (Elliott, 1982; Leipper, 1970; Vukovich, 2007). Studies of spawning Atlantic bluefin tuna (ABT) show that their larvae are associated with the edges of anticyclonic eddies that spin off from the Loop Current (Lindo-Atichati *et al.*, 2012; Muhling *et al.*, 2013; Teo *et al.*, 2007). While anticyclonic eddies are downwelling features, their edges have been shown to be associated with higher production, depending upon feature age (Biggs, 1992; Salas-de-León *et al.*, 2004; Wang *et al.*, 2018). They could therefore represent more favorable local habitats for larval fish feeding and development, implying different phytoplankton assemblages and food-web characteristics than expected for oligotrophic oceanic waters.

The goal of the present study was to characterize the phytoplankton community associated with these eddy edges in the GoM at the time of ABT spawning. We used a combination of flow cytometry, microscopy and high performance liquid chromatography (HPLC) pigment analyses on two expeditions conducted in May of consecutive years, during the peak time of ABT spawning. We assess biomass, composition and size structure of the phytoplankton community in profiles that covered the depth range of the euphotic zone and thus also compare assemblages, carbon (C) biomass and C:Chl ratios in the mixed layer (ML) and the deep chlorophyll maximum (DCM). While we found few obvious correlations between ABT larvae and phytoplankton community properties, we compare our GoM sites to Hawaii Ocean Time-series (HOT) and Bermuda Atlantic Times-series Study (BATS) sites as all are nitrogen-limited, oligotrophic, land-remote, warm, deep-water picoplankton-dominated systems.

METHOD

Sampling

Two research expeditions were conducted aboard the NOAA Ship *Nancy Foste*r in May 2017 (NF1704) and May 2018 (NF1802) during the peak month of ABT larval abundance (Lindo-Atichati *et al.*, 2012; Muhling *et al.*, 2013; Teo *et al.*, 2007). Station locations were chosen based on habitat characteristics known to be associated with ABT larvae (Domingues *et al.*, 2016; Muhling *et al.*, 2013), detailed by Gerard *et al.* (2021). Once a suitable location was found, we initiated a multi-day experiment, hereafter called *cycle* (Landry *et al.*, 2009), consisting of daily intensive sampling with CTD profiles and net tows, *in situ* incubation experiments, and a sediment trap deployment, following a satellite-tracked drift array. Table I lists the abbreviations for variables referred to in this study.

Samples for most phytoplankton-related parameters were collected pre-dawn from Niskin bottles mounted on a 24-place rosette system equipped with a Seabird SBE911 CTD and a Seapoint fluorometer. Fluorescence data (volts) from the fluorometer was compared with discrete bottle data analyzed with HPLC (Pigments section) to convert the voltage data to total chlorophyll *a* (*T*CHL*a*) equivalents for the purpose of obtaining *T*CHL*a* integrals deeper than the bottle data allowed.

Same-day noon CTD casts were also conducted to collect *Trichodesmium* (Microscopy section) and to determine *in situ* light levels (%incident light or $\%I_0$) of photosynthetically active radiation (PAR) at the depths of water collection on the pre-dawn cast. The PAR sensor, a Biospherical Instruments QSP-2300, was mounted on the top of the CTD rosette frame. Five cycles were completed; however, the PAR sensor was inoperable during Cycle 2

Table I: Abbreviations used for variables referred to in this study

ABT: Atlanticnbluefin tuna	ML: mixed layer
AC: autotrophic carbon, includes cyanobacteria and eukaryotic phytoplankton	MVCHL*a*: monovinyl chlorophyll *a*
A-DINO: dinoflagellates	MVCHL*b*: monvinyl chlorophyll *b*
A-EUK: autotrophic eukaryotes	NEO: neoxanthin
ALLO: allophycocyanin	NCF: normalized chlorophyll fluorescence
BATS: Bermuda Atlantic Times-series Study	NF1704: May 2017 expedition
BUT: 19′-but-fucoxanthin	NF1802: May 2018 expedition
C#: Cycle number, C1-C3 were during NF1704; C4-C5 were during NF1802	NPP: Net Primary Production
C:CHL: carbon:chlorophyll (μg C L^{-1}: μg CHL L^{-1})	PAR: Photosynthetically Active Radiation
CHL: total chlorophyll *a*, sum of MVCHL*a* and DVCHL*a*	PELAG: pelagophytes
CHLc*3*: chlorophyll *c3*	PER: peridinin
CHLOR: chlorophytes	PEUK: mainly ≤2 μm eukaryotic phytoplankton from flow cytometry
CRYPT: cryptophytes	PRAS*3*: prasinophytes—type 3
DCM: deep chlorophyll maximum	PRAS: prasinoxanthin
DIAT: diatoms	PRO: *Prochlorococcus*
DVCHL*a*: divinyl chlorophyll *a*	PRYM: prymnesiophytes—type 6
FCM: flow cytometry	SYN: *Synechococcus*
FUCO: fucoxanthin	*T*CHL*a*: total chlorophyll *a* (sum of MVCHL*a* and DVCHL*a*)
HEX: 19′-hex-fucoxanthin	*T*CHL*b*: total chlorophyll *b* (sum of MVCHL*b* and DVCHL*b*)
HOT: Hawaii Ocean Time-series	TRICH: *Trichodesmium*
HPLC: high-pressure liquid chromatography	ZEAX: zeaxanthin

(C2) of NF1704 and C5 of NF1802, so sample depths were chosen with CTD fluorometer fluorescence values best matching previously determined *in situ* light levels.

Flow cytometry

Picophytoplankton abundances were estimated by flow cytometry (FCM) from preserved (0.5% paraformaldehyde) 2-mL samples, frozen in LN_2, then stored at −80°C. Samples were thawed and stained for 1 h with the DNA stain Hoechst 33342 (1 μg ml^{-1}, (Monger and Landry, 1993)), then analyzed with a Beckman Coulter EPICS Altra flow cytometer (Selph *et al.*, 2011). Listmode data were processed using FlowJo (version 9.7.7, Treestar, Inc.) to delineate *Prochlorococcus* (PRO), *Synechococcus* (SYN) and eukaryotic phytoplankton (PEUK). PRO and SYN abundances were converted to carbon using 32 and 101 fg C $cell^{-1}$, respectively (Brown *et al.*, 2008; Garrison *et al.*, 2000). PEUK were mainly ≤2 μm cells; however, we subtract microscopic counts for cells from 2 to 5 μm, and the remaining cells were converted to carbon and scaled to be that of a cell twice the diameter of SYN (808 fg C $cell^{-1}$).

The sum of abundance-weighted normalized chlorophyll fluorescence (NCF) was significantly correlated with *T*CHL*a* fluorescence (Supplementary Fig. 1, NF1704 $r^2 = 0.96$; NF1802 $r^2 = 0.94$), as shown in other data sets (Li *et al.*, 1993; Zettler *et al.*, 1996). Thus, the NCF from PRO, SYN and PEUK and their abundances were used to partition the total FCM chlorophyll fluorescence into the relative contributions of these groups;

$$(1)\quad \text{PRO NCF L}^{-1} = \text{PRO NCF} \times \text{PRO}\ \left(\text{cells L}^{-1}\right)$$

$$(2)\quad \text{SYN NCF L}^{-1} = \text{SYN NCF} \times \text{SYN}\ \left(\text{cells L}^{-1}\right)$$

$$(3)\quad \text{PEUK NCF L}^{-1} = \text{PEUK NCF} \times \text{PEUK}\ \left(\text{cells L}^{-1}\right)$$

Assuming that PRO NCF L^{-1} was directly proportional to the pigment divinyl chlorophyll *a* (DVCHL*a*, ng L^{-1}) since DVCHL*a* is only found in PRO, we estimated the monovinyl chlorophyll *a* (MVCHL*a*) associated with SYN as:

$$(4)\quad \textit{S}\text{YN MVChla} = \frac{\text{SYN NCF L}^{-1}}{\text{PRO NCF L}^{-1}} \times \text{DVChla}$$

SYN MVCHL*a* was subtracted from the total MVCHL*a*, as was the contribution of *Trichodesmium* (TRICH, Microscopy section), and the remaining MVCHL*a* was used for all eukaryotic taxa in the CHEMTAX analyses (Pigments section).

Pigments

Samples (2.2-L) were collected for pigment analyses by HPLC at the Horn Point Analytical Services Laboratory (University of Maryland Center for Environmental Science). They were filtered onto GF/F filters, frozen in LN_2 and stored at −85°C until extracted, and analyzed using an automated 1100 HPLC system with Agilent temperature-controlled autosampler, Peltier temperature-controlled column oven compartment, PDA detector and ChemStation software. The HPLC method uses a C8 column and a reversed phase, methanol-based solvent

system (Hooker *et al.*, 2012; Van Heukelem and Thomas, 2001). MVCHL*a* and DVCHL*a* are detected at 665 nm. Carotenoid and xanthophyll accessory pigments are detected at 450 nm.

The pigments used for phytoplankton taxonomic identification were MVCHL*a* and DVCHL*a* (sum = *T*CHL*a*), monovinyl chlorophyll *b* (MVCHL*b*), divinyl chlorophyll *b* (DVCHL*b*), chlorophyll *c3* (CHL*c3*), zeaxanthin (ZEAX), fucoxanthin (FUCO), 19′-hexfucoxanthin (HEX), 19′-but-fucoxanthin (BUT), allophycocyanin (ALLO), peridinin (PER), neoxanthin (NEO) and prasinoxanthin (PRAS). Since CHL*a* contributions for PRO and SYN were assigned from FCM (above) and contributions of TRICH were based on microscopical analyses (below), all pigments, except for DVCHL*a* and ZEAX, were entered into the CHEMTAX program (v. 1.95 (Wright, 2008)), for partitioning into eukaryotic groups.

Initial pigment ratios (accessory pigment: MVCHL*a*) used in CHEMTAX were those of oceanic species (Higgens *et al.*, 2011) and indicative of the following groups: chlorophytes (CHLOR), diatoms (DIAT), prymnesiophytes—type 6 (PRYM), pelagophytes (PELAG), cryptophytes (CRYPT), prasinophytes—type 3 (PRAS*3*) and dinoflagellates (A-DINO). Data were divided into two groups: shallower and deeper than 60 m, since some of the accessory pigments were only present in deep samples (NEO and ALLO) and the general pattern of pigments showed a different community at depth. The initial ratio matrix was randomized into 60 matrices (×0.7 random number between −0.5 and +0.5), which were then applied to the data sets (Supplementary Table I).

Microscopy

The microscopical analyses presented here are from the top two depths (~80%I_0 and 40%I_0) and the bottom 2 depths (~5%I_0 and 1%I_0) sampled, a subset of the total data set (4/11 stations during NF1704; 6/10 stations during NF1802), and are used to characterize the nano- and micro-phytoplankton community, and to validate the relative contributions of eukaryotic groups to MVCHL*a* using CHEMTAX (Pigments section). Microscope slides were prepared from 500 mL of preserved sample (260 μL alkaline Lugol's solution (0.1% final), 10 mL 10% buffered formalin, 500 μL 3% sodium thiosulfate; modified protocol from (Sherr and Sherr, 1993)), to which 1 mL 0.33% proflavine (w/v) and 1 mL of 4′,6-diamidino-2-phenylindole (DAPI, 0.01 mg mL^{-1}) were added. For analysis of cells < 10-μm, a slide was prepared from 50 mL subsamples filtered onto a 25-mm, 0.8-μm pore size, black PCTE filter and mounted on a glass slide. For larger (10- to ~50-μm) cells, the remaining sample was filtered onto a 25-mm, 8-μm pore size, black PCTE filter. Slides were frozen (−80°C) until image analysis as detailed in Taylor *et al.*, (2015) Cell biovolumes (BV, μm^3) were calculated according to Taylor *et al.* (2011). BV was converted to carbon (C, pg $cell^{-1}$) using $C = 0.216 \times BV^{0.939}$ for non-diatoms and $C = 0.288 \times BV^{0.811}$ for diatoms (Menden-Deuer and Lessard, 2000).

Imaged phytoplankton cells were grouped into size categories by cell lengths of 2–5, 5–10, 10–20, and > 20-μm. "Autotrophs" were identified based on the presence of chlorophyll (CHL); however, some were also likely to use heterotrophic nutrition (i.e. mixotrophs). Phytoplankton taxonomic structure was assessed to the extent possible, separating cells into A-DINO, diatoms and unidentified flagellates. The FCM-derived PEUK abundance, once 2–5 μm cells from microscopy were subtracted, represented cells ≤ 2 μm (not counted with microscopy), and their carbon contents were added to the microscope slide-estimated carbon for a total phytoplankton community carbon estimate. These data were also used to determine carbon: chlorophyll (C:CHL) ratios at the depths where both measurements were taken. Missing intermediate depths (for carbon) were estimated using the 5%I_0 C:CHL ratio.

TRICH abundances were assessed from 6.6-L samples taken from 6 depths (2–50 m) in daily (~noon) CTD casts. Water was gravity filtered directly from the Niskin bottle onto 8-μm, 47-mm Millipore TETP filters, preserved (2% paraformaldehyde), mounted on glass slides and frozen (−80°C). Thawed filters were scanned using a dissecting microscope (10X-30X) with a NightSea SFA adaptor and Royal Blue light head (EX 440–460 nm, EM > 500 nm) to find all orange-glowing trichomes and colonies. TRICH were digitally imaged (OMAX camera) using ToupLite (Touptec.com), counted and trichome lengths measured. Trichome widths were determined with an Olympus BX-41 epifluorescence microscope (200X, EX 450–480 nm, dichroic 500 nm, EM > 515 nm). These data comprised the background contribution of trichomes to HPLC samples (Pigments section). Colony and tuft volumes were estimated by dividing their width by the mean trichome width to get the number of trichomes per colony, with colony volume equal to the single trichome volume times the number of trichomes per colony.

Trichome CHL, carbon and nitrogen (CN) contents to biovolume ratios were determined from 6.6-L samples collected as above on the same noon casts but onto 20-μm, 47-mm filters and frozen (−80°C). Individual TRICH were suspended in salt water and duplicate samples taken for CHL, CN and biovolume. The CHL fraction was filtered onto GF/F filters, extracted (90% acetone) and

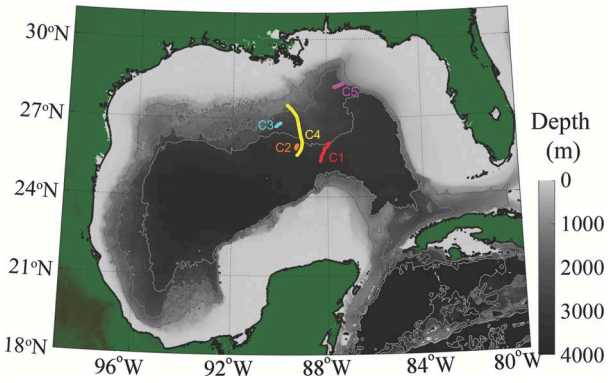

Fig. 1. Map of cycle locations during NF1702 and NF1802. Table II lists coordinates (latitude/longitude) and dates of occupation for each station within each cycle (C1-C5).

fluorescence determined with a 10 AU fluorometer using the acidification method (Strickland and Parsons, 1972). For elemental analyses, samples were analyzed at the UC Santa Cruz Stable Isotope Laboratory with a Carlo Erba 1108. Biovolumes from microscopic examination were converted to carbon using the generated C: biovolume ratio.

Statistical analyses

All statistical analyses (i.e. *t*-test for comparing means with equal or unequal variances, single factor analysis of variance) were performed with the data analysis package of Microsoft Excel for Mac, ver. 16.16.22. In the text, data are listed as averages ±1 standard deviation of the mean; in figures, error bars represent ±1 standard error of the mean to better fit the estimates of variance on the figures.

RESULTS

Five cycles of 2- to 4-day duration (referred to by cycle number and sample day, e.g. cycle 1, Day 1 is C1.1), were conducted on cruises NF1704 (May 2017) and NF1802 (May 2018) (Fig. 1). C1–C3 were in the deep waters of the Mexico Basin (Love *et al.*, 2013), with bottom depths of 2675–3388 m (Table II). C4 was also in the Mexico Basin, near the Mississippi Slope with bottom depth of 1559 m but drifting over deeper waters of 3344 m. C5 was conducted at the deep-water edge of the Florida Escarpment, off the northern West Florida Shelf with bottom depths of 1862–2619 m. C1 and C5 contained abundant larval ABT, whereas C2 and C3 had no larvae and C4 had very few (Gerard *et al.*, 2021).

C1-C3 showed similar euphotic zone temperature-salinity (T-S) properties within each cycle, whereas C4 and C5 were more variable (Fig. 2). C4.1 salinity was lower in the upper 50 m relative to later cycle days (i.e. 0–20 m salinity of <36.40 in C4.1 versus 36.42 in C4.2). Between 50–125 m, C4.1–4 were similar, whereas C4.5 was colder from 100 to 125 m. C5.1-C5.2 had the same T-S properties, whereas C5.3–5 varied depending upon the amount of fresh water entrained (salinities of 35.46–36.37 at ≤20 m versus ∼36.50 at 40–50 m).

Mixed layer (ML) depths ranged from 21 to 36 m during NF1704 (C1-C3) and 11–27 m during NF1802 (C4-C5, Table II). The DCM ranged from ∼97–139 m during C1-C3 and 69–120 m during C4-C5. Larval ABT were abundant during cycles with shallower DCMs (∼100 m and 69–88 m, in C1 and C5, respectively). During NF1704, the depth of the $1\%I_0$ generally coincided with, or was slightly shallower than, the DCM; however, during NF1802, their relative positions were variable (Table II).

To present results below, we first outline the cyanobacteria component of the phytoplankton community, followed by the eukaryotic component. Phytoplankton size classes and pigment-based taxonomy are presented next, along with C:CHL ratios. Details of the pigment data and CHEMTAX outputs are provided in Supplementary Tables II-IX.

Prokaryotic phytoplankton

PRO biomass during C1–C4 showed a subsurface maximum at ∼80 m, while for C5 it was at 60–80 m (Fig. 3). DVCHL*a* and PRO biomass increased with depth until ∼80 m, from where biomass stayed constant or decreased, while DVCHL*a* increased. C5 variances were high, reflecting euphotic zone depth differences (Table II). SYN MVCHL*a* and biomass were much lower than PRO and DVCHL*a* except in C5, where ML SYN were similar to PRO (Fig. 3). C5 deeper samples had higher PRO than SYN, as in other cycles.

Euphotic-zone integrated biomass of PRO was relatively invariant within cruises (Fig. 4), but was significantly lower for NF1802 ($P < .05$), averaging 532 ± 61 mg C m^{-2} (NF1704) and 315 ± 75 mg C m^{-2} (NF1802). SYN biomass averaged 68 ± 6 mg C m^{-2} and 124 ± 20 mg C m^{-2}, for NF1704 and NF1802, respectively, and was significantly higher during NF1802 ($P < 0.05$).

TRICH had a biovolume: CHL ratio of 2.16×10^9 μm^3 μg^{-1}, a biovolume: C ratio of 6.62×10^6 μm^3 μg C^{-1}, and a C:CHL ratio of 327 (data not shown). Mean C: N (g: g) was 5.6 ($n = 2$). Average trichome length and width was 2.63 ± 1.68 mm ($n = 1337$) and 16.1 ± 3.0 μm ($n = 17$), respectively, yielding 0.25 ± 0.16 ng CHL

Table II: Stations occupied aboard the expeditions (EXP.) aboard the NOAA ship Nancy Foster in the Gulf of Mexico during NF1704 (11–30 May 2017) and NF1802 (5–19 May 2018)

EXP.	CYCLE.DAY	DATE	LAT (°N)	LON (°W)	Bottom depth (m)	Surface Temp. (°C)	MLD Depth (m)	DCM Depth (m)	1%I_0 Depth (m)
NF1704	C1.1	5/11/17	26.0523	87.8539	3045	24.5	30	98	100
	C1.2	5/12/17	25.9270	88.0107	3080	24.6	31	100	100
	C1.3	5/13/17	25.7200	88.1505	3201	24.6	36	97	nd
	C1.4	5/14/17	25.4064	88.2693	3388	24.9	21	102	nd
	C2.1	5/16/17	25.9923	89.2522	3156	25.3	26	116	nd
	C2.2	5/17/17	25.9162	89.3308	3190	25.5	24	108	nd
	C2.3	5/18/17	25.8552	89.3228	3233	25.6	23	135	nd
	C3.1	5/27/17	26.6339	90.1794	2802	26.6	33	133	129
	C3.2	5/28/17	26.7235	90.1196	2725	26.9	22	141	124
	C3.3	5/29/17	26.7837	90.0419	2691	26.9	30	136	nd
	C3.4	5/30/17	26.8138	89.9787	2675	27.0	26	139	nd
NF1802	C4.1	5/05/18	27.4918	89.6769	1559	25.4	20	115	115
	C4.2	5/06/18	27.0512	89.3445	2470	25.5	22	104	110
	C4.3	5/07/18	26.3830	89.1247	2914	25.6	27	120	109
	C4.4	5/08/18	25.9348	89.0624	3119	25.9	26	118	88
	C4.5	5/09/18	25.5428	89.2894	3344	25.9	23	88	74
	C5.1	5/15/18	28.2258	87.3032	1862	25.2	13	86	78
	C5.2	5/16/18	28.2606	87.4507	2619	25.3	13	84	94
	C5.3	5/17/18	28.2127	87.5327	2537	25.6	11	80	91
	C5.4	5/18/18	28.1896	87.6254	2592	25.7	14	69	85
	C5.5	5/19/18	28.1649	87.6981	2524	26.0	11	69	nd

Shown are the cycles (C1-C5), and each day of station occupation (Cycle.Day), occupation date (M/D/Y), location (latitude (LAT)/longitude (LON)), bottom depth (m), surface temperature (°C), mixed layer depth (MLD, m, Δ0.1 kg m^{-3} from 10 m criterion), depth (m) of the DCM and 1% Io (i.e. 1% of incident PAR irradiance). For many stations, the PAR meter was inoperable, so "nd" indicates casts where no data exists for I_0.

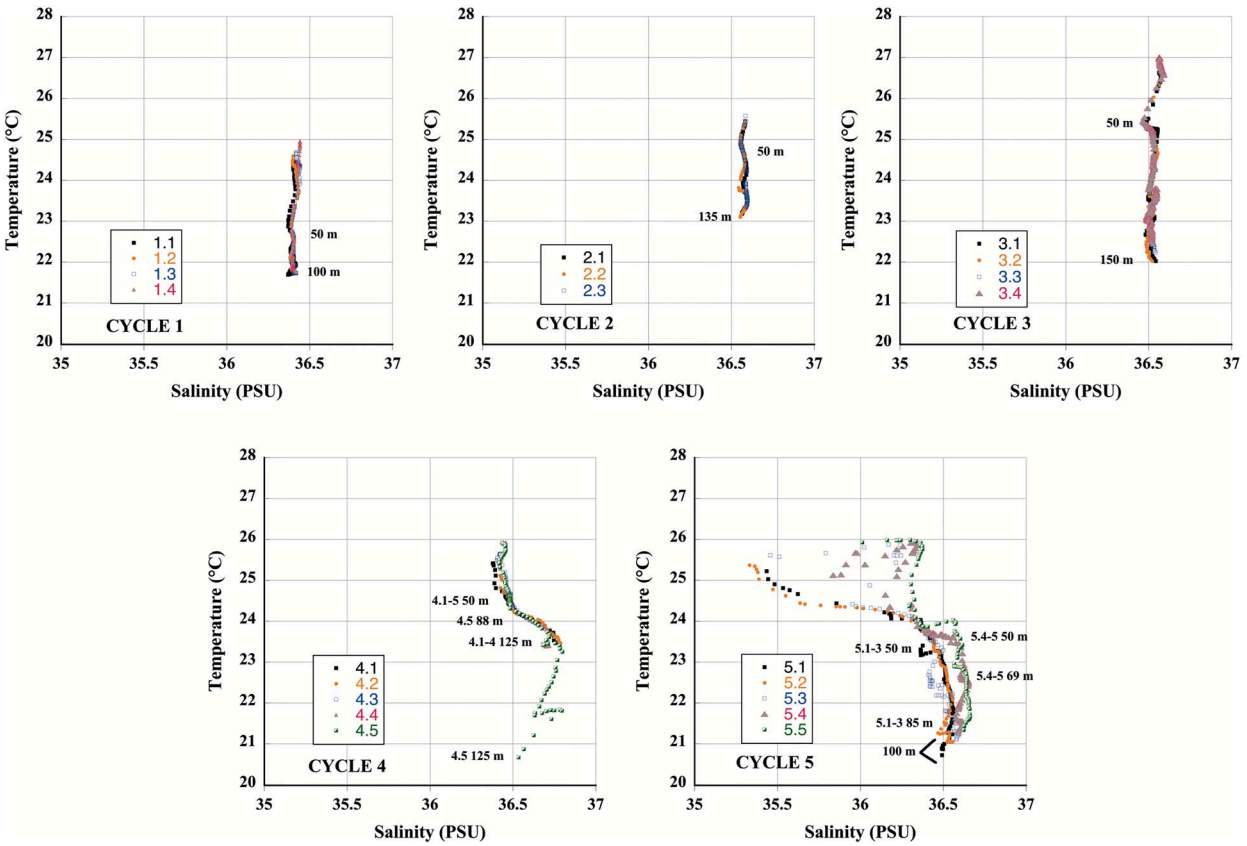

Fig. 2. Temperature-Salinity (T-S) plots of the euphotic zone of Cycles 1–5. Indicated on each plot are the T-S at 50 m and the deepest T-S plotted for that Cycle.Day.

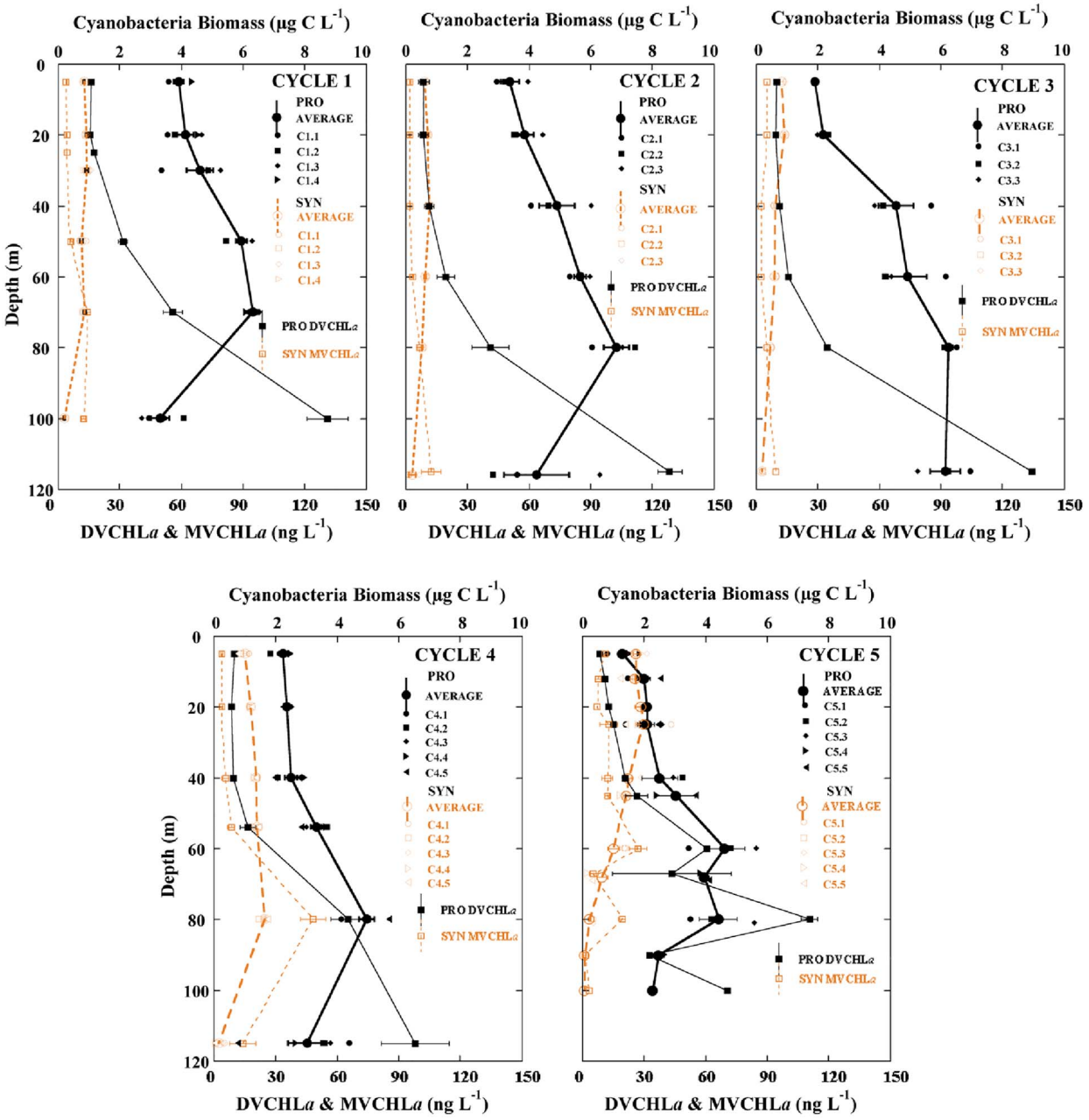

Fig. 3. Depth profiles of PRO and SYN biomass (µg C L^{-1}) for each cycle, as well as DVCHL*a* and SYN-associated MVCHL*a* (ng L^{-1}). Average values (±1 standard error) of all stations within a cycle are shown as lines (solid, black for PRO, dashed, orange for SYN) for all populations and cycles.

trichome^{-1}. TRICH colony CHL content was 22.4 ± 26.4 ng CHL (n = 116, NF1704) and 48.2 ± 64.8 ng CHL (n = 7, NF1802).

TRICH had a patchy distribution, with some 2.2-L HPLC samples including single colonies (3 of 28 in the upper 50 m), but overall in the 6.6-L samples examined for NF1704 (n = 45), they averaged only 0.4 colonies L^{-1}. Fig. 4 shows the background TRICH biomass, excluding colonies. TRICH biomass was 7-fold higher during NF1704 than NF1802 (10 ± 6 versus 1.4 ± 1.7 mg C m^{-2}, respectively), but always much lower than other cyanobacterial groups.

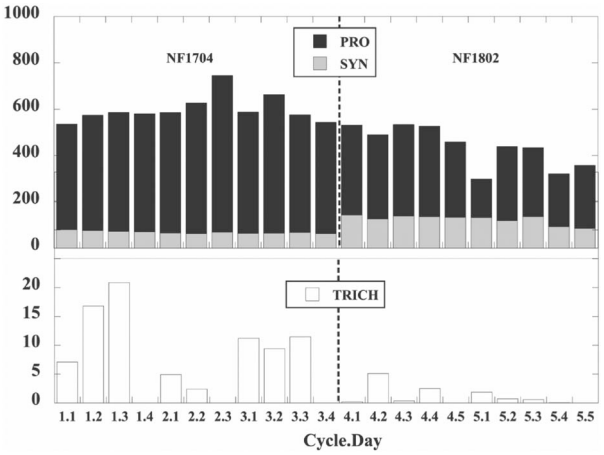

Fig. 4. Euphotic zone-integrated cyanobacteria biomass (mg C m^{-2}) from flow cytometry and microscopy for each cycle sampling day (surface to 1% incident light level, except to 1.5% Io for C3). Cyanobacteria are comprised of PRO, SYN and TRICH. Note change in *y*-axis scale between TRICH and PRO/SYN plots.

Eukaryotic phytoplankton

Pigment depth profiles for C1 clearly showed a DCM maximum (Fig. 5), with ML (5–30 m) concentrations of 16.2 ± 1.2 ng DVCHL*a* L^{-1} and 31.8 ± 5.6 ng MVCHL*a* L^{-1} (Table III), and DCM (100 m) values of 131.2 ± 19.9 ng DVCHL*a* L^{-1} and 220.4 ± 18.3 ng MVCHL*a* L^{-1} (Table IV). ML MVCHL*a* values were similar for C1, C3 and C5, but C2 and C4 were ∼30% less. HEX was the dominant accessory pigment (C1 ML: 4.5 ± 0.9 ng L^{-1}; DCM: 71.1 ± 14.6 ng L^{-1}), with most HEX attributed to PRYM (Fig. 5), but some in PELAG (Supplementary Table I). MVCHL*b* was also relatively high in the DCM (59.8 ± 10.6 ng L^{-1}), but low in the ML (1.3 ± 1.2 ng L^{-1}). BUT, associated mostly with PELAG (but some in PRYM, Supp. Table I), was 1.3 ± 0.3 ng L^{-1} in ML waters and 40.4 ± 10.7 ng L^{-1} at 100 m. FUCO, PER and PRAS, attributed to DIAT, A-DINO and PRAS*3*, respectively, were all low in the ML (≤1 ng L^{-1}) but increased in the DCM (6–10 ng L^{-1}, Fig. 5). ALLO (CRYPT) was only present in deep waters (2 ng L^{-1}). Results for other cycles, which had only minor differences from C1, are discussed in the context of *T*CHL*a*, below, as are the taxon-specific distributions of MVCHL*a*. Further details of HPLC pigment results are available in Supplementary Tables II-IX.

Autotrophic carbon

Total euphotic zone integrated values of autotrophic carbon (AC) from FCM and microscopy ranged from 463 to 1,268 mg C m^{-2} for C1, C4 and C5, the only cycles were all populations were measured (Table V). AC was highest during C1 (1,097 ± 177 mg C m^{-2}), while C4 and C5 had similar AC of 805 ± 132 and 750 ± 257 mg C m^{-2}, respectively. C5.1 had the lowest AC (463 mg C m^{-2}), whereas C5.5 had the highest < 2 μm PEUK of 314 mg C m^{-2}, likely reflecting the high proportions of PRYM and PRAS*3* at this station (Table IV). For C1 and C5, ∼50% of AC occurred in autotrophic eukaryotes (A-EUK), whereas A-EUK were only 33% in C4. Cyanobacteria (PRO + SYN) accounted for 35–78% of total AC, averaging 52, 67 and 48% for C1, C4 and C5, respectively. Microscopically-determined A-EUK were mostly smaller flagellates, including A-DINO, with few DIAT (data not shown).

Euphotic zone average ratios of C:CHL (C1, C4 and C5) were 117 ± 58, with the highest ratio for C1 (132 ± 56) and the lowest for C5 (97 ± 43, Fig. 6). ML C:CHL ratios were higher (171 ± 38) than at the DCM (39 ± 16). C:CHL of ML PRO always exceeded A-EUK, but became more equal with depth, as PRO C:CHL decreased faster than A-EUK C:CHL.

Total phytoplankton community

Euphotic-zone integrated *T*CHL*a* was similar in NF1704 and NF1802 (10.3 ± 2.2 and 10.4 ± 1.9 mg m^{-2}, respectively), as was MVCHL*a* (5.9 ± 1.7 versus 6.7 ± 1.8 mg m^{-2}) (Fig 6). However, DVCHL*a* was significantly lower during NF1802 (3.7 ± 1.0 mg m^{-2}) than NF1704 (4.4 ± 0.5 mg m^{-2}, $P = .04$). In addition, MVCHL*a* was significantly higher at stations where ABT larvae were abundant (C1 and C5) relative to where they were not ($P < .004$), but DVCHL*a* was not different between these cycles ($P > .05$).

CTD-mounted fluorometer voltage was calibrated against HPLC bottle data (Supplementary Fig. 2), resulting in 0–175 m integrals of 18.3 ± 2.8 and 18.5 ± 3.6 mg *T*CHL*a* m^{-2} for NF1704 and NF1802, respectively (Fig. 7). C4.5 had the lowest *T*CHLa (11.6 mg m^{-2}), after the DCM shoaled 30 m relative to the previous day.

During both cruises, PRO and SYN comprised ∼41% of ML *T*CHL*a*, while TRICH was ∼1% (Table III). Pico and nano-eukaryotic phytoplankton were dominated by PRYM (∼39% *T*CHL*a*), followed by CHLOR (8%) and PELAG (4%). SYN increased from 9 to 17% of *T*CHL*a* from NF1704 to NF1802; however, no other significant cruise differences were observed in the ML. Larger microphytoplankton comprised a consistently small percentage of ML biomass (∼6% for A-DINO and DIAT combined).

In the DCM, cyanobacteria accounted for 62% of *T*CHL*a* during NF1704, dropping to 36% during NF1802 (Table IV). This mainly reflects the lower DVCHL*a* percentage of *T*CHL*a* during NF1802 (32%) versus NF1704 (56%). SYN comprised 3% of DCM

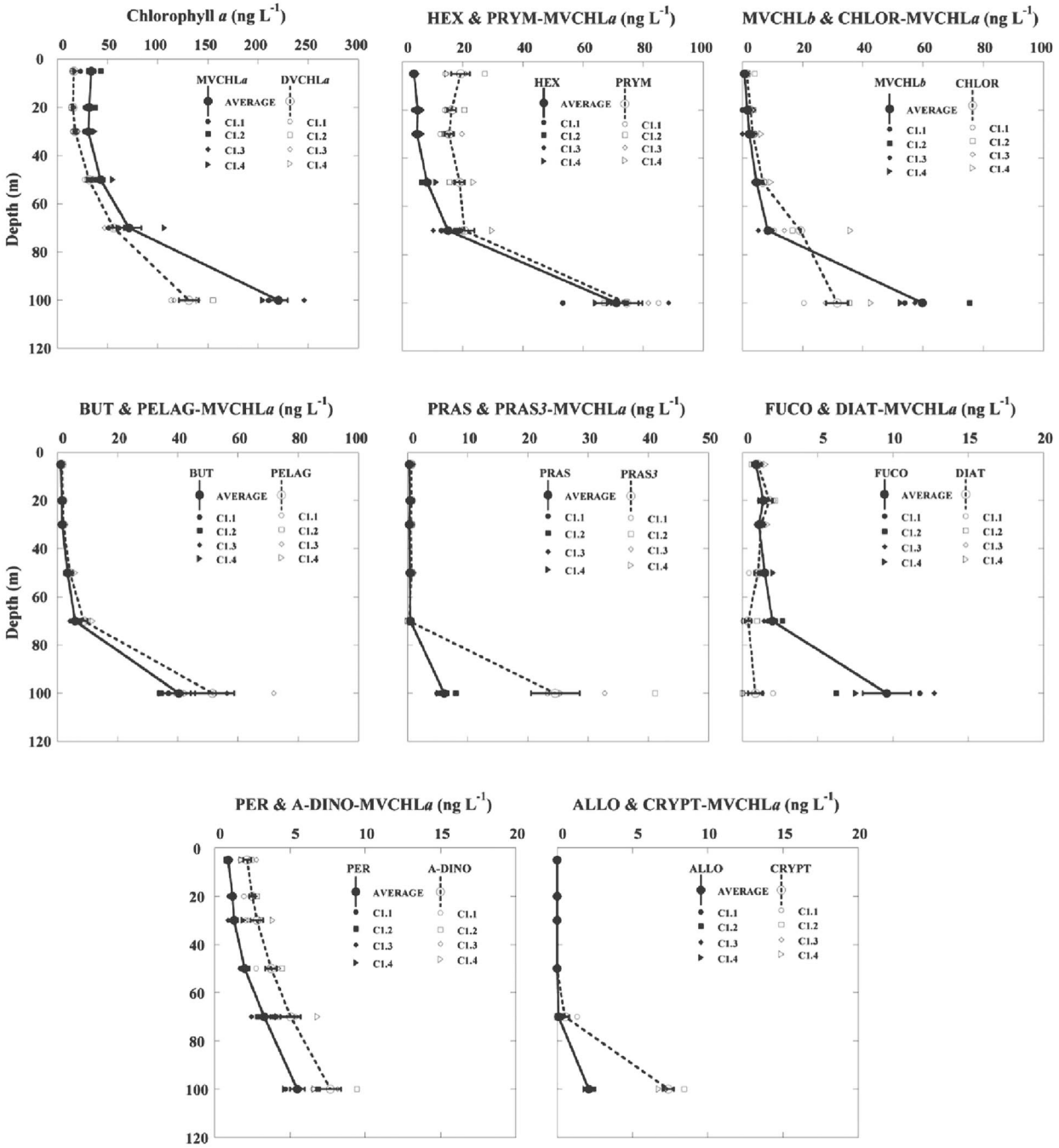

Fig. 5. Depth profiles of Cycle 1 (C1) HPLC pigments (ng L^{-1}) and CHEMTAX assignments of taxonomic groups (ng MVCHL*a* L^{-1}). Shown are the within-cycle station average ±1 standard error of stations 1.1 to 1.4. Solid lines are for pigments; dashed lines for taxa, except for DVCHL*a*, which is also dashed. Note differences in x-axis scaling.

*T*CHL*a* during C1 and ~0.3–7% during C4-C5, except in the much shallower DCM of C4.5, where SYN was 29% of *T*CHL*a* (Table II).

As in the ML, PRYM was the dominant eukaryotic group at the DCM; however, they only represented 16 and 29% of *T*CHL*a* during NF1704 and NF1802, respectively (Table IV). PELAG accounted for 9% of *T*CHL*a* during both cruises, while CHLOR dropped from 8 to 4% between NF1704 and NF1802. A-DINO and DIAT were 1–3% of *T*CHL*a* for both cruises, while PRAS*3* (3

Table III: Pigments (ng L-1) are from HPLC determinations, and taxonomic assignments (indicated in bold lettering) are from CHEMTAX (ng MVCHLa L-1)

Cycle.Day	*n*	MVCHL*a*	DVCHL*a*	HEX	BUT	FUCO	PER	MVCHL*b*	PRAS
C1.1–4	11	31.8 ± 5.6	16.2 ± 1.2	4.5 ± 0.9	1.3 ± 0.3	1.1 ± 0.3	1.1 ± 0.2	1.3 ± 1.2	0.3 ± 0.1
C2.1–3	6	20.3 ± 3.7	8.6 ± 1.3	2.9 ± 0.8	0.9 ± 0.3	0.8 ± 0.3	0.7 ± 0.1	1.2 ± 0.9	0.3 ± 0.03
C3.1	2	29.7 ± 7.3	9.7 ± 0.3	2.3 ± 0.04	0.6 ± 0.04	0.5 ± 0.1	0.7 ± 0.0	1.4 ± 0.01	0.3 ± 0.03
C4.1–5	9	20.5 ± 2.9	9.6 ± 2.2	3.2 ± 0.6	0.7 ± 0.2	0.7 ± 0.2	0.6 ± 0.2	1.4 ± 0.3	0
C5.1–5	10	35.9 ± 8.6	10.0 ± 2.9	6.5 ± 2.7	1.9 ± 2.6	0.8 ± 0.3	1.0 ± 0.2	3.1 ± 0.8	0.4 ± 0.1
Cycle.Day	**SYN**	**TRICH**	**PRYM**	**PELAG**	**DIAT**	**A-DINO**	**CHLOR**	**PRAS*3***	
C1.1–4	4.1 ± 0.3	1.2 ± 1.8	17.2 ± 4.4	1.7 ± 0.3	1.3 ± 0.5	2.4 ± 0.5	2.8 ± 2.2	0.8 ± 0.1	
C2.1–3	2.0 ± 0.5	0.1 ± 0.1	11.9 ± 2.8	12.0 ± 0.4	0.9 ± 0.7	1.6 ± 0.3	2.1 ± 1.6	0.6 ± 0.2	
C3.1	5.2 ± 0.1	0.8 ± 0.5	17.0 ± 5.3	1.0 ± 0.1	0.3 ± 0.1	1.6 ± 0.2	3.1 ± 0.8	0.7 ± 0.1	
C4.1–5	3.8 ± 1.2	0.4 ± 0.5	10.7 ± 2.7	0.9 ± 0.2	0.7 ± 0.4	1.2 ± 0.5	2.8 ± 0.7	0	
C5.1–5	9.2 ± 3.2	0.04 ± 0.1	17.2 ± 6.1	2.2 ± 2.6	0.2 ± 0.2	1.8 ± 0.5	4.3 ± 1.3	0.8 ± 0.2	

Data are averages ± standard deviation of samples in the mixed layer (change in 0.1 kg m^{-3} from density at 10 m), with the number of observations (*n*) for each cycle indicated. Pigments (ng L^{-1}) are from HPLC determinations, and taxonomic assignments are from CHEMTAX (ng MVCHL*a* L^{-1}). Pigments and taxa abbreviations are defined in the text.

Table IV: Deep pigment and taxonomic assignments for each cycle

Cycle.Day	*n*	Depth (m)	MVCHL*a*	DVCHL*a*	HEX	BUT	FUCO	PER	MVCHL*b*	PRAS	ALLO
C1.1–4	4	100	220.4 ± 18.3	131.2 ± 19.9	71.1 ± 14.6	40.4 ± 10.7	9.6 ± 3.2	5.5 ± 1.0	59.8 ± 10.6	6.1 ± 1.4	2.1 ± 0.2
C2.1–2	2	116	129.9 ± 4.7	133.6 ± 0	52.9 ± 4.2	26.6 ± 2.8	4.1 ± 0.2	2.3 ± 0.4	21.4 ± 4.7	1.4 ± 0.4	0.2 ± 0.3
C2.3	1	115[a]	58.6	118.2	17.3	6.8	1.6	1.2	15.5	0.3	0.6
C3.1	1	115[a]	59.3	134.5	15.9	7.2	1.4	1.7	16.9	0.3	0
C4.1–4	4	104–120	145.0 ± 7.5	114.2 ± 10.6	46.9 ± 9.4	19.2 ± 3.6	7.1 ± 2.0	1.3 ± 0.3	18.0 ± 4.6	1.6 ± 0.3	10.1 ± 1.5
C4.5	1	80	140.4	87.4	41.8	15.9	7.3	3.0	22.7	2.0	1.1
C5.1	1	80	241.1	105.4	73.8	38.0	19.9	3.3	52.6	6.7	11.2
C5.2	1	80	191.9	108.1	71.1	19.0	11.3	4.7	43.9	3.6	0
C5.3	1	81	171.7	118.3	41.2	8.3	4.0	3.0	56.3	5.8	10.6
C5.4	1	67	295.2	72.5	73.5	14.4	5.5	6.1	135.3	17.7	4.6
C5.5	1	69	163.2	31.8	107.5	24.3	12.5	6.5	111.2	16.7	3.2
Cycle.Day	**SYN**	**PRYM**	**PELAG**	**DIAT**	**A-DINO**	**CHLOR**	**PRAS*3***	**CRYPT**			
C1.1–4	12.5 ± 2.0	74.5 ± 10.4	51.6 ± 14.6	0.9 ± 1.0	7.7 ± 1.4	35.1 ± 10.9	30.7 ± 8.1	7.4 ± 0.7			
C2.1–2	7.7 ± 2.5	64.1 ± 5.0	31.2 ± 3.4	0	3.0 ± 0.5	17.8 ± 2.5	5.3 ± 4.7	0.9 ± 1.2			
C2.3[a]	21.4	17.1	6.9	0	1.4	9.4	0.8	1.6			
C3.1[a]	9.4	20.5	8.4	0	2.0	18.6	0.5	0.1			
C4.1–4	17.1 ± 14.1	60.6 ± 13.2	25.5 ± 5.3	1.1 ± 0.8	1.8 ± 0.4	0.6 ± 0.6	5.0 ± 1.2	33.3 ± 4.4			
C4.5	65.4	40.5	17.2	2.5	3.4	0.3	8.4	2.8			
C5.1	22.6	83.5	46.9	13.0	4.1	2.4	33.6	35.1			
C5.2	17.0	93.3	26.1	4.1	6.5	24.1	20.7	0.1[b]			
C5.3	18.6	64.5	12.9	0	4.2	14.0	22.2	35.4			
C5.4	7.5	127.2	23.6	0	8.9	30.2	80.7	17.1			
C5.5	3.2	64.9	18.0	3.5	6.0	0	52.0	6.4			

Data are averages ± standard deviation of samples at the DCM, with the number of observations (*n*) for each cycle indicated. Pigments (ng L^{-1}) are from HPLC determinations, and taxonomic assignments are from CHEMTAX (ng MVCHL*a* L^{-1}). Pigments and taxa abbreviations are defined in the text.

[a]The sampling depths for C2.3 and C3.1 was shallower than the ~133 m DCM, at ~115 m.

[b]Indicates highest value of CRYPT (20.6 ng L^{-1}) is at 100 m, not the 82 m DCM.

to 13%) and CRYPT (1 to 7%) increased from NF1704 to NF1802. DCM depth was correlated with %*T*CHL*a* at the DCM for only 3 taxa: PRO, PRYM and PRAS*3* (Fig. 8). PRO increased with deepening DCMs, whereas PRYM and PRAS*3* decreased.

Taxon-specific distributions of AC showed clear differences between ML and DCM communities (Fig. 9). Within-cycle taxonomic differences were coincident with euphotic zone depth. Hence, C4.5 and C5.4–5 were very different from the earlier days of these cycles, as their euphotic zone depths were 11–30 m shallower (Table II). AC was 1.4–2.7-fold higher in the DCM relative to the ML. In all cycles, ML biomass was dominated by PRO, PRYM and SYN (83–92% of total AC). In the DCM, PRO and PRYM still dominated the phytoplankton community (48–80% of AC), but PELAG, CHLOR, CRYPT, PRAS*3* or SYN contributed significantly at different stations.

Table V: Euphotic zone integrated estimates of autotrophic phytoplankton biomass (mg Cm^{-2}) from combined epifluorescence microscopy and flow cytometry during C1, C4 and C5. Cycle averages (AVG) for each biomass fraction are indicated in bold.

Cycle.Day	<2 μm CYANO	<2 μm PEUK	2–5	5–10	10–20	20–40	>40	Total
C1.1	532	65	142	93	11	7	0	849
C1.2	567	83	193	259	23	8	8	1,141
C1.3	605	71	191	340	21	20	20	1,268
C1.4	572	72	115	323	27	21	0	1,129
C1 AVG	**569**	**73**	**160**	**254**	**21**	**14**	**7**	**1,097**
C4.1	528	52	60	23	12	5	1	681
C4.3	565	60	69	56	16	14	12	792
C4.5	514	51	182	137	28	21	10	943
C4 AVG	**536**	**54**	**104**	**72**	**19**	**13**	**8**	**805**
C5.1	306	60	44	36	5	3	8	463
C5.3	446	79	140	129	12	12	7	827
C5.5	339	314	140	135	16	16	1	960
C5 AVG	**364**	**151**	**108**	**100**	**11**	**10**	**5**	**750**

Data are subdivided into size (cell diameter) classes as follows: <2 μm CYANO (PRO and SYN from flow cytometry), <2 μm PEUK (picoeukaryotes from flow cytometry), and the remaining categories (μm, cell diameter) from epifluorescence microscopy (2–5, 5–10, 10–20, 20–40, >40 μm and total of all size classes).

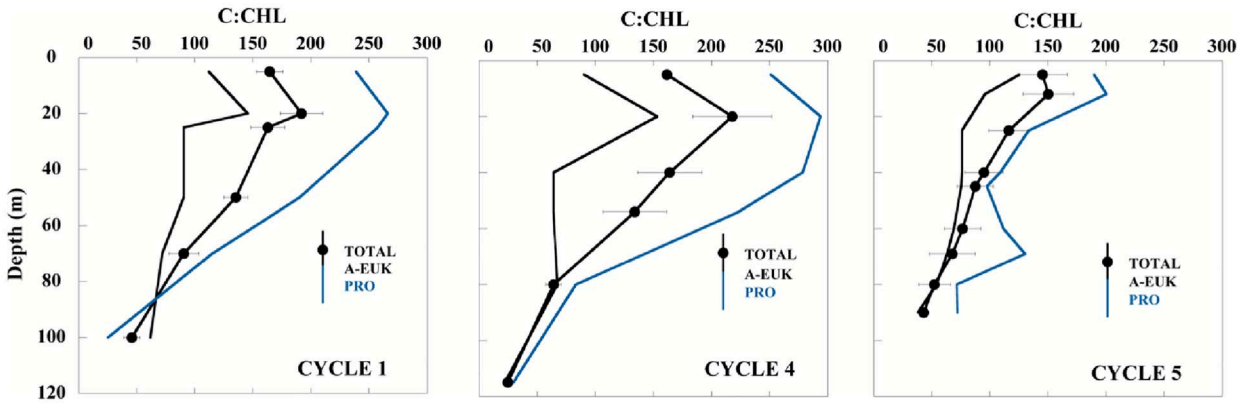

Fig. 6. Depth profiles of carbon: chlorophyll (C:CHL, by weight) ratios for the total phytoplankton community (TOTAL, filled symbols), phototrophic eukaryotes (A-EUK) and PRO in C1, C4 and C5, where HPLC MVCHL*a* and DVCHL*a* was measured as well as microscopy/flow cytometry-based carbon. Uncertainties are standard errors of mean estimates for TOTAL C:CHL.

*T*CHL*a* from the CTD-mounted fluorometer shows the full depth range of the DCM, as well as highlighting differences among cycle days (Fig. 10). C1 showed subsurface biomass maxima, with PRO+SYN at ~ 70 m and A-EUK at 100 m, in the middle of the DCM feature. For C4, subsurface biomass maxima were present except for A-EUK in C4.1–4, where the DCM covered a broad depth range (~100–130 m) and the A-EUK maxima may have been missed. In C5, the A-EUK maxima were near the top of DCM, while PRO+SYN maxima were 10–20 m shallower.

DISCUSSION

In the discussion sections below, we first outline our methodological approach to determine the community composition of the phytoplankton in the oligotrophic GoM, and the advantage of this approach over alternative methods. We follow this with a brief description of our study sites in terms of their physical–chemical properties, then outline our main pigment and carbon-based findings. Finally, these phytoplankton communities of the coastally-enclosed oceanic GoM are compared and contrasted to other land-remote oligotrophic regions.

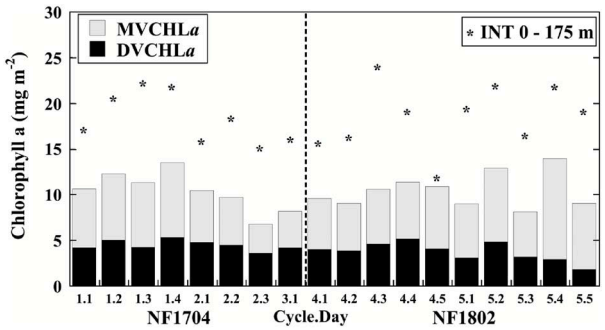

Fig. 7. Euphotic zone-integrated MVCHL*a* and DVCHL*a* at each station (mg Chl m^{-2}, bars), along with integrals (0–175 m) of *T*CHL*a* from the CTD-mounted profiling fluorometer (* symbols). Station locations are described in Table II. The euphotic zone comprises depths to the 1% incident light level (1% I_o), except to 1.5% I_o for C3.1.

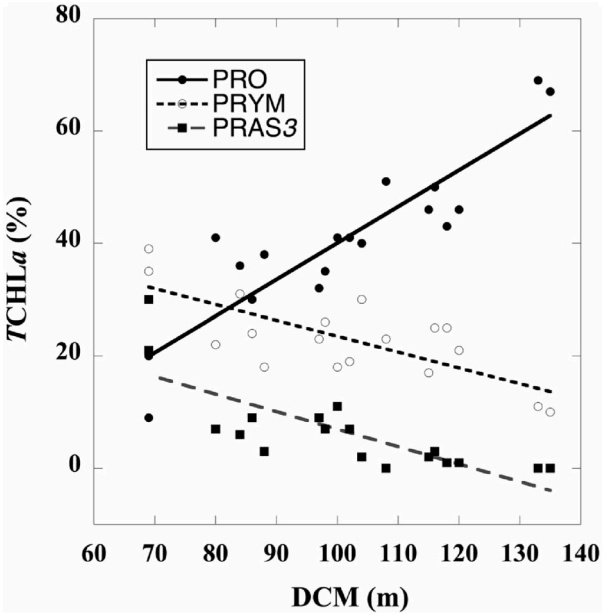

Fig. 8. Fraction of *T*CHL*a* (%) as a function of DCM depth (m) for PRO, PRYM and prasinophytes (PRAS*3*) at the DCM depth. Linear regressions are: $Y = -24.8 + 0.65X$, $r^2 = 0.80$ (PRO); $Y = 51.7–0.28X$, $r^2 = 0.54$ (PRYM); $Y = 38.1–0.31X$, $r^2 = 0.60$ (PRAS*3*).

Methodology

Most phytoplankton data in models of the oceanic GoM come from satellite measurements of ocean color (e.g. (Biggs and Ressler, 2001; Gomez *et al.*, 2018; Martínez-López and Zavala-Hidalgo, 2009; Müller-Karger *et al.*, 2015)). However, models based on ocean color and biogeochemical ocean circulation may underestimate depth-integrated net primary production (NPP) versus *in situ* data (Friedrichs *et al.*, 2009; Saba *et al.*, 2010), although those accounting for dominant taxa (Aiken *et al.*, 2008; Uitz *et al.*, 2010) or using backscatter to estimate phytoplankton carbon may have better fits (Westberry *et al.*, 2008). This is due in part to satellites sensing only surface chlorophyll concentrations, with an assumed vertical structure. For our data set, C1 and C5 had nearly identical ML *T*CHL*a* (48 and 46.9 ng L^{-1}, respectively), but very different biomass profiles, NPP and taxonomic compositions in the ML and DCM (Landry *et al.*, 2021), showing the limitation of such an approach. Thus, even though more costly and time intensive, studies that incorporate *in situ* sampling are not entirely replaceable by purely remote methodology.

We combined data from three independent, complementary methods (FCM, HPLC and microscopy) to obtain depth-resolved phytoplankton community composition over the deep waters of the GoM. Together, these methods allow estimates of phytoplankton carbon biomass, useful as a common currency for understanding carbon transformations between trophic levels. PRO and SYN carbon were derived from conservative (low end) cell conversions, representative of oligotrophic regions (Brown *et al.*, 2008; Shalapyonok *et al.*, 2001; Veldhuis and Kraay, 2004; Worden *et al.*, 2004) at pre-dawn sampling times when PRO biomass is typically a daily minimum (Claustre *et al.*, 2002; Liu *et al.*, 1997; Mann and Chisholm, 2000; Vaulot *et al.*, 1995). For TRICH and the heterogeneous (in shape and size) eukaryote assemblage, we used direct measurements (TRICH) or microscopy-derived cell biovolumes combined with carbon conversions from the literature (eukaryotes). Total AC was partitioned into HPLC-defined A-EUK taxa assuming that each group's carbon equaled its contribution to MVCHL*a*. Our approach produced a unique data set of taxon-specific, C-biomass estimates for the full phytoplankton community over the depth range of the euphotic zone for this region. These data provide the foundation for assessing major flows of carbon from primary producers to other trophic levels (Landry *et al.*, 2021; Landry and Swalethorp, 2021; Stukel *et al.*, 2021a) or as remineralized and exported production (Kelly *et al.*, 2021; Stukel *et al.*, 2021b, Yingling *et al.*, 2021).

FINDINGS

Each cycle followed a 15-m drogued drift array enabling daily quasi-Lagrangian sampling of a moving parcel of water. Sampling in NF1704 (C1-C3) was in the Mexico Basin, with T-S properties within a cycle suggesting that we were following the same water parcel. For NF1802, C4 started on the edge of the Mississippi Slope, and followed the drift array southward over the Mexico Basin with T-S properties largely coherent until C4.5, when temperature at depth became colder and DCM depth shoaled dramatically. C5 started on the edge of the Florida Escarpment

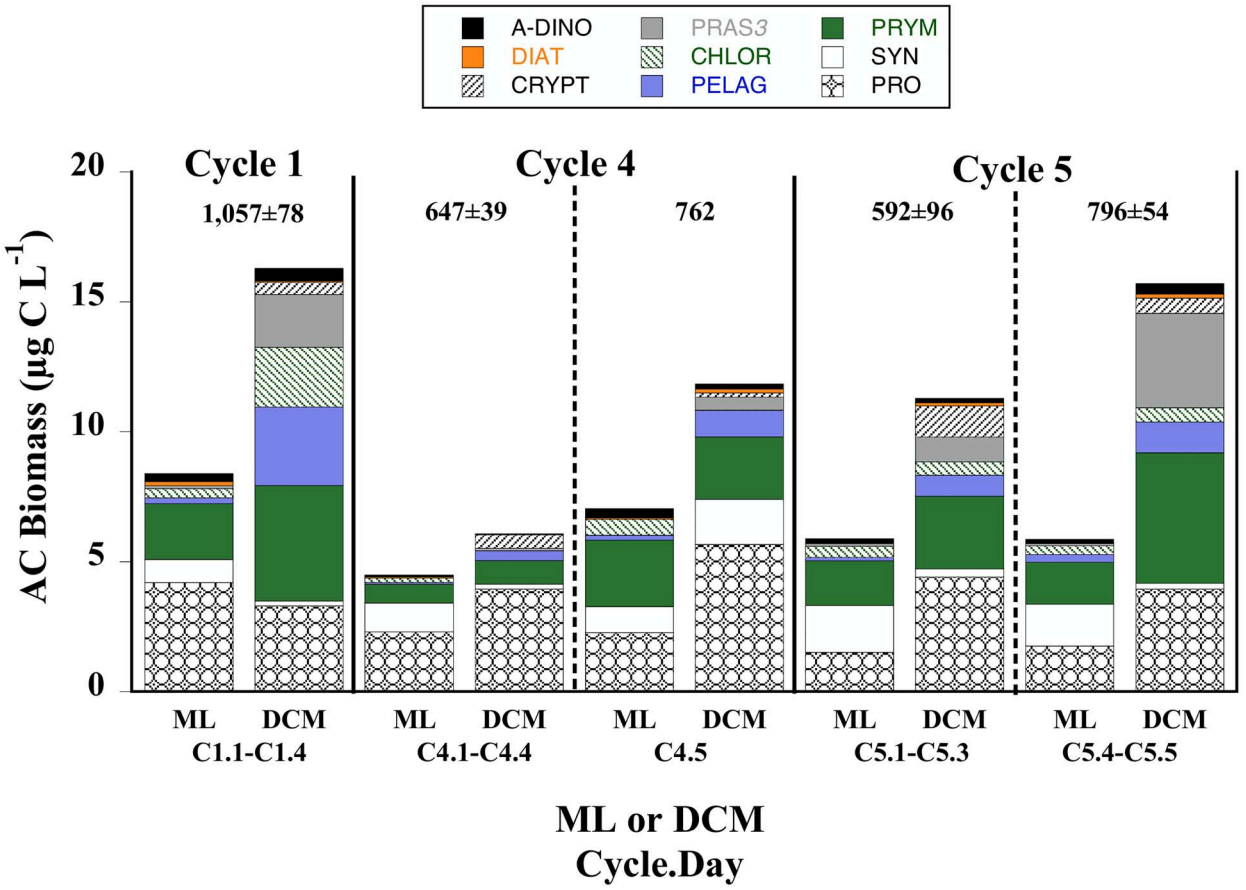

Fig. 9. AC biomass (µg C L^{-1}) partitioned into taxonomic groups. Data shown are mean values for the ML and DCM. Above each set of data (and below the cycle no.) is the total mean ± 1 standard error of the euphotic zone integrated AC biomass (mg m^{-2}). C1 data are means of all days, C4 is divided into means for days 1 to 4 (C4.1–4) and Day 5 (C4.5), and C5 is divided into means of days 1 to 3 (C5.1–3) and Days 4 and 5 (C5.4–5).

with fresher surface water, which mixed with saltier water as the cycle progressed. Deeper waters of C5 showed smaller increases in salinity that varied with cycle day, while DCMs gradually shoaled from 88 to 69 m. Backward trajectory analyses of surface waters (2 week intervals) showed a coastal influence of ABT larvae-containing C1 and C5 waters, with C5 waters more recently in a higher nutrient area, whereas waters in the other cycles (where ABT larvae were few or absent) were in deep GoM waters without coastal influence 2 weeks prior to sampling (Gerard *et al.*, 2021).

Nitrate plus nitrite was generally ≤0.1 µM in the upper 100 m of NF1704 (Knapp *et al.*, 2021). However, C1.1 and C1.3 saw slightly higher 100-m values of 0.3 µM, which is reflected in their shallower DCMs. C2 and C3 both had deeper nitraclines (>120 m). The nitracline was ~100 m through most of C4, but the shallower DCM at C4.5 indicates a nitracline closer to 80 m. During C5, the nitracline was ≤80 m (Knapp *et al.*, 2021). These results are consistent with previous studies, where nitrate and phosphate were usually <0.1 µM in the euphotic zone (Biggs and Ressler, 2001; Jochens and DiMarco, 2008). Kelly *et al.* (2021) showed that vertical diffusion of nitrate into the lower euphotic zone was higher during C4 and C5 relative to C1-C3; however, the increase was significant only for C5 and still represented a very low vertical nitrate flux. Indeed, Kelly *et al.* (2021) suggested that lateral transport of organic matter into our study region may supply most of the new nitrogen used to fuel export, although phytoplankton were primarily relying on ammonia regenerated from this organic matter (Yingling *et al.*, 2021). Also, the abrupt topography of the Florida Escarpment may have induced vertical motions in the water column, bringing more nutrients to the euphotic zone (Hidalgo-González and Alvarez-Borrego, 2008; Sansón and Provenzale, 2009). For phytoplankton community comparisons, we treat C4.5 separately from C4.1–4, and C5.1–3 separately from C5.4–5 because of their different

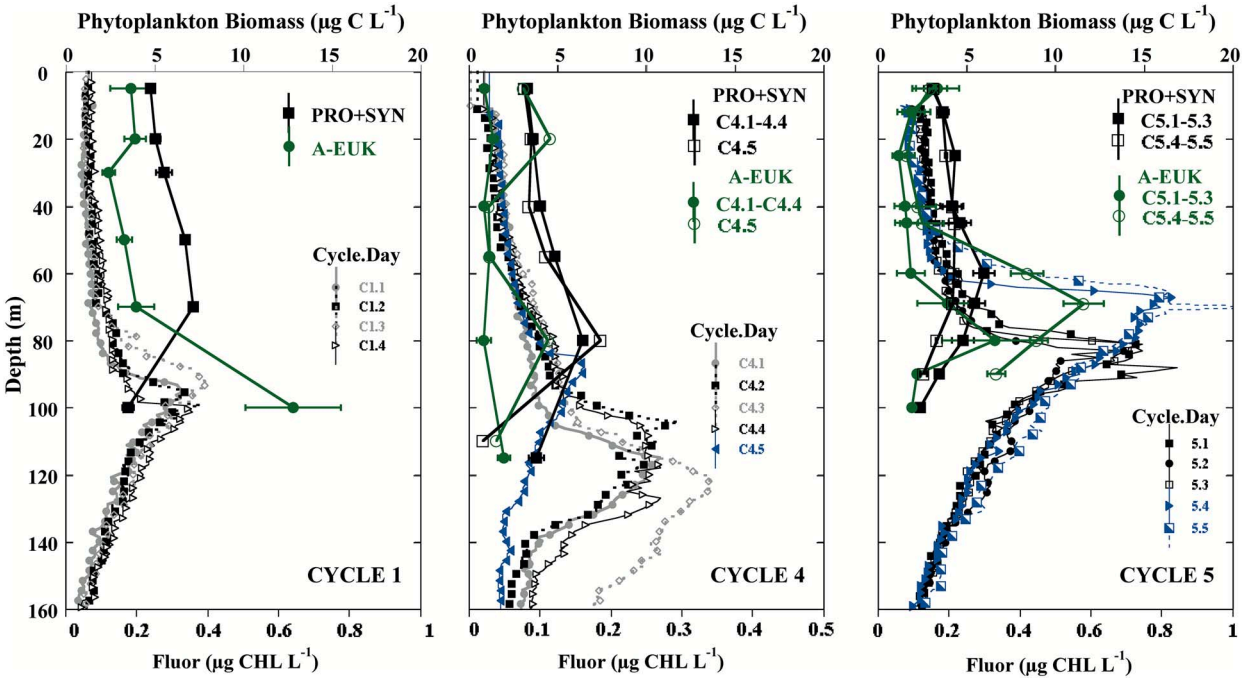

Fig. 10. Depth profiles of phytoplankton biomass (µg C L^{-1}) as total A-EUK and prokaryotes (PRO + SYN) in C1, C4 and C5, overlain on continuous profiles of chlorophyll fluorescence from CTD-mounted instrument for same casts (Fluor, µg CHL L^{-1}). Data are within-cycle averages ±1 standard error. Note change in Fluor *x*-axis in C4 (0–0.5 versus 0–1 µg CHL L^{-1} for C1/C5).

euphotic zone depths (~84 versus 69 m, respectively), which are viewed as proxies for the nitracline (Richardson and Bendtsen, 2019).

Phytoplankton pigment and biomass distributions

We found significant contributions of DVCHL*a* to *T*CHL*a*, but over half was MVCHL*a*. In all cycles, submesoscale differences in surface (ML) phytoplankton taxa were small. For both cruises, the major diagnostic pigments (and their associated taxa) were DVCHL*a* (PRO), HEX (PRYM), BUT (PELAG) and MVCHL*b* (CHLOR). FUCO (DIAT) and PER (A-DINO) were always less than 5% of *T*CHL*a*. ML pigment concentrations were quite low, and the main taxa were PRO, PRYM and SYN. Phytoplankton biomass was dominated by PRO and PRYM, accounting for 55–76% of AC, followed by SYN of 11–30% of AC. Nutrient uptake experiments showed that ML phytoplankton were primarily relying on recycled ammonia, suggesting that high ammonia affinity was important to these taxa (Yingling *et al.*, 2021). For C1-C3, phytoplankton pigment compositions showed no obvious temporal trends, suggesting that the populations were in quasi-steady state. Despite the slightly fresher C4.1, all C4 days had similar ML phytoplankton compositions, as was true for the C5 ML samples despite more mixing.

TRICH comprised only ~1% of total MVCHL*a* in the upper 50 m, although it can be important episodically in the GoM, especially later in the summer when wet deposition of Fe through Saharan dust may encourage its growth (Holl *et al.*, 2007; Lenes *et al.*, 2012; Mulholland *et al.*, 2006; Walsh and Steidinger, 2001). TRICH trichomes had an average CHL content of 0.25 ± 0.16 ng, which is equal to the 0.27 ng CHL trichome^{-1} found by Carpenter et al. (2004) in the Atlantic Ocean.

Pigment concentrations were consistently higher in the DCM and appeared to change with nitracline depth. AC biomass was ~2-fold higher in the DCM than in the ML, following the trends in pigment concentration. While PRO and PRYM still dominated the DCM (47–80% of AC), a more diverse taxa (CHLOR, PELAG) were present, and some cycles had detectable concentrations of PRAS*3* and CRYPT. These differences likely reflected changes in nutrient availability as the nitracline shoaled or deepened. For instance, PRO, PRYM and PELAG were similar between days in C4, until C4.5, where the shallower DCM contained 22% more SYN and 12% less CRYPT relative to earlier days. During C5, the DCM shoaled from 86 to 69 m between C5.1–3 and C5.4–5, with C5.4–5 having ~50% lower PRO, 3-fold

more PRAS*3*, and somewhat more PRYM (35% versus 22–33% in C5.1–3). These differences explain the positive trends of PRO with DCM depth and the negative trends for PRYM and PRAS*3* (Fig. 9). The overall greater abundance of A-EUK at the DCM coincided with a higher proportion of nitrate utilized at this depth, although ammonia was still the dominant nutrient source (Yingling, *et al.*, 2021).

Our data suggest that higher euphotic zone nutrients (shallower nitracline depths) in NF1802 relative to NF1704 led to differences in PRO and SYN abundances between cruises. We found DVCHL*a* (PRO) was ~30% lower during NF1802, while SYN was significantly higher. We can infer that PRO is associated with lower nutrient concentrations, while PRYM and PRAS*3* dominate as more nutrients become available. Latasa *et al.* (2010, 2016) examined relative distributions of DCM phytoplankton and found PRO associated with oligotrophic waters, while SYN, PRYM and PELAG clustered together as a mesotrophic group, and DIAT, A-DINO, CHLOR, CRYPT and PRAS*3* were associated with eutrophic conditions. In our study, we found CRYPT only at the DCM, and its presence increased greatly in NF1802, suggesting more nutrients during that cruise. We found no increase in DIAT during NF1802, which is consistent with the relatively deep depth (>150 m) of the "silicline" in GoM waters (Barbero *et al.*, 2019; Jochens and DiMarco, 2008; Morrison and Nowlin, 1977).

We found C:CHL ratios of 171 ± 38 in the ML and 39 ± 16 at the DCM with a depth-integrated average of 80 ± 16. These results are consistent with phytoplankton having lower CHL content under the high light and nitrogen limitation conditions of near-surface waters (Eppley *et al.*, 1971; Geider, 1987; Morgan and Kalff, 1979; Riemann *et al.*, 1989). PRO DVCHL*a*, a significant fraction of *T*CHL*a*, increased 7-fold from 0.14 ± 0.05 fg cell^{-1} in the ML, to 0.99 ± 0.38 fg cell^{-1} at the DCM, also showing the expected negative correlation of light and DVCHL*a* content (Bouman *et al.*, 2006; Partensky *et al.*, 1996; Veldhuis and Kraay, 2004).

Due to cycle differences in C:CHL ratios for specific taxa, trends were subtly different between pigments and carbon biomass. For instance, PRYM was the dominant A-EUK taxa in terms of pigments and biomass in all cycles, but its integrated C:CHL ratio varied (81 ± 20, 59 ± 13 and 69 ± 27 for C1, C4 and C5, respectively). Thus, PRYM AC was twice as high (223 mg C m^{-2}) in C1 versus C4 and C5 (76 and 138 mg C m^{-2}, respectively), despite having a similar amount of MVCHL*a*. Along with lower PRYM biomass in C4 and C5 relative to C1, lower growth rates resulted in lower PRYM production on the 2018 cruise (Landry *et al.*, 2021). Similarly, PRO biomass was higher in C1 (493 mg C m^{-2}) versus C4 and C5 (385 and 254 mg C m^{-2}, respectively), but PRO growth was low during C1, resulting in higher PRO production in the latter cycles (Landry *et al.*, 2021). These results highlight the need for measurements of phytoplankton pigment, carbon biomass and growth rates to fully understand taxon-specific contributions to primary production and food-web fluxes.

Comparisons to other areas

As an oligotrophic, nitrogen-limited, deep-water habitat, the oceanic GoM has characteristics that can be compared to the North Pacific Subtropical Gyre (NPSG) HOT and the BATS sites. There is much more seasonal mixing and energetic eddy activity at BATS than HOT, creating seasonal pulses of export production at BATS versus persistent dominance of regenerated production at HOT (Brix *et al.*, 2006; Roman *et al.*, 2001). In the GoM, the large influence of the Loop Current and seasonal inputs of riverine waters to the shelf edges are dimensions of variability not seen at the remote open-ocean sites. In the discussion below, we focus on FCM cell abundances and HPLC pigment concentrations, as these are measurements of phytoplankton composition and biomass that we have in common with HOT and BATS (Table VI).

While NPP is similar between HOT and BATS (13.1–13.9 mol m^{-2} y^{-1}, (Brix *et al.*, 2006)), the BATS phytoplankton community is more variable than at HOT. BATS has regular spring blooms of all taxa, with only occasional diatom blooms (Krause *et al.*, 2009; Steinberg *et al.*, 2001), explaining its higher and more variable pigment means in surface and deeper waters (Table VI). Also, SYN at HOT averages $0.2 \pm 0.2 \times 10^{12}$ cells m^{-2}, whereas it ranges widely at BATS from 0.3 to 3.0×10^{12} cells m^{-2}. During spring bloom periods at BATS, SYN abundance exceeds PRO, while PRO exceeds SYN during summer and autumn (DuRand *et al.*, 2001). In contrast, ML PRO at HOT is always ~30-fold higher than SYN, and PRO varies little annually, while SYN is somewhat higher in the winter (Pasulka *et al.*, 2013).

Comparing between locations, GoM PRO (9.8–16.6×10^{12} cells m^{-2}) was within the range of values found at BATS, but lower than at HOT (Table VI). GoM integrated PRO: SYN abundance decreased 3-fold between cruises because of decreases in PRO coinciding with increases in SYN abundance. However, because we sampled in the center of the Mexico Basin in 2017 and close to the edges of it in 2018, these differences could just reflect location, as opposed to inherent variability. With regard to pigments, the largest difference in pigment concentration between HOT and GoM is the ratio of DVCHL*a*: MVCHL*a* of 1.36 for HOT versus 0.55–0.74 for the GoM, consistent with the higher concentration of

Table VI: Comparison of open ocean oligotrophic GoM to HOT and BATS data sets

Integrals	HOT	BATS	GoM NF1704	GoM NF1802		
[a]PRO ($\times 10^{12}$ cells m^{-2})	24.7 ± 3.9	1–20	16.6 ± 1.9	9.8 ± 2.4		
[a]SYN ($\times 10^{12}$ cells m^{-2})	0.2 ± 0.1	0.3–3	0.7 ± 0.1	1.2 ± 0.2		
[b]*T*CHL*a* (mg m^{-2})	26.3 ± 4.0 (103)	23.8 ± 8.3 (135)	18.3 ± 2.8 (8)	18.5 ± 3.6 (10)		
[b]MVCHL*a* (mg m^{-2})	11.2 ± 3.5 (103)	nd	5.9 ± 1.7 (8)	6.7 ± 1.8 (10)		
[b] DVCHL*a* (mg m^{-2})	15.2 ± 3.0 (103)	nd	4.4 ± 0.5 (8)	3.7 ± 1.0 (10)		
Pigments	**HOT**	**BATS Surface (ng L^{-1})**	**GoM**	**HOT**	**BATS DCM (ng L^{-1})**	**GoM**
Depth range		0–30 m		73–150 m	57–142 m	69–141 m
Mean DCM		110 ± 15	92 ± 20	107 ± 22		
No. observations	200	409	39	103	146	18
*T*CHL*a*	81.8 ± 28.7	99.6 ± 102.6	40.1 ± 10.9	310.4 ± 55.0	309.2 ± 105.8	273.3 ± 75.7
[c]MVCHL*a*	36.6 ± 13.9	nd	34.7 ± 22.5	122.9 ± 54.0	nd	164.7 ± 65.2
[c,d]DVCHL*a*	45.2 ± 22.2	nd	11.7 ± 3.9	187.5 ± 42.5	nd	108.6 ± 35.6
*T*CHL*b*	8.8 ± 8.9	12.3 ± 17.2	2.4 ± 1.7	139.5 ± 48.7	100.5 ± 56.4	147.5 ± 42.4
BUT	4.4 ± 2.9	11.6 ± 12.8	1.2 ± 1.4	40.2 ± 14.8	54.3 ± 33.1	23.6 ± 12.8
FUCO	4.6 ± 1.8	6.1 ± 8.2	0.9 ± 0.3	7.0 ± 3.4	13.6 ± 14.7	7.6 ± 4.7
HEX	12.0 ± 4.8	29.9 ± 30.2	4.4 ± 2.1	64.4 ± 17.7	95.4 ± 39.9	55.8 ± 24.2
[e]PER	0.8 ± 0.6	1.6 ± 2.3	0.9 ± 0.3	2.0 ± 2.0	3.7 ± 3.7	3.4 ± 2.0
PRAS	0.02 ± 0.12	1.3 ± 3.7	0.3 ± 0.2	0.6 ± 1.2	4.8 ± 7.0	4.8 ± 5.1

HOT PRO, SYN and HPLC pigment data are from HOT cruises 199–307 (Jan 2008-Nov 2018). BATS pigment data are from BATS cruises 231–366 (Jan 2008-Dec 2019). BATS PRO and SYN data are from DuRand *et al.* (2001) and Malmstrom *et al.* (2010). Pigment abbreviations defined in Table I. Uncertainties are standard deviations of mean estimates, with the number of observations in parentheses; "nd" indicates parameter not determined.

[a]PRO and SYN integrals are 0–200 m for HOT and BATS, but only to the 1%I_0 depth for the GoM.

[b]TCHLa is a 0–175 m integral for all locations; however, MVCHLa and DVCHLa are 0–175 m for HOT and only to 1%I_0 depth for the GoM.

[c]BATS HPLC data do not distinguish between MVCHLa and DVCHLa.

[d]GoM MVCHLa is significantly higher in NF1704 versus NF1802 ($P < .05$).

[e]BATS PER data omits Jan-July 2008 cruises as it was anomalously high.

PRO at HOT versus the GoM. While DVCHL*a* is not measured at BATS, we can infer that it would be lower than HOT assuming similar pigment: cell contents.

On our GoM cruises, bottle samples were taken down to the base of euphotic zone at 1%I_0 (Ryther, 1956), which captured the bulk of phytoplankton carbon. However, in oligotrophic waters with very deep chlorophyll maxima, the compensation depth (depth where NPP equals zero) is often closer to 0.3%I_0 (Cullen and Eppley, 1981; Marra *et al.*, 2014). Therefore, it is not surprising that *T*CHL*a* (from the profiling CTD fluorometer) was almost twice as high integrated to 175 m (~0.1%I_0, 18.4 ± 3.2 mg m^{-2}, Table VI) versus the bottle data estimate to 1%I_0 (10 mg m^{-2}). The GoM 0–175 m integral is ~30% lower than the annual mean at HOT, but within the error of the mean at BATS (26.3 ± 4.0 and 23.8 ± 8.3 mg m^{-2}, respectively).

HEX is used widely as an indicator pigment for PRYM and has been found to dominate A-EUK taxa throughout oligotrophic ocean sites, including HOT and BATS (Goericke, 1998; Letelier *et al.*, 1993; Rii *et al.*, 2016; Steinberg *et al.*, 2001; Veldhuis and Kraay, 2004) and the oligotrophic offshore/slope waters of the northern GoM (Chakraborty and Lohrenz, 2015; Qian *et al.*, 2003). In contrast, on the inner shelf and coastal areas of the northern GOM, elevated nutrients and freshwater favor DIAT over PRYM (Qian *et al.*, 2003). As HEX (PRYM) was the dominant A-EUK pigment (taxon) in both our ML and DCM samples, and DIAT were always low in our samples, we conclude that the phytoplankton community data reported here are representative of the deep water GoM, rather than coastal or shelf areas.

GoM surface (0–30 m) *T*CHL*a* and accessory pigments were much lower than at HOT and BATS (Table VI). However, the BATS data are highly variable (>100% coefficient of variation), encompassing the GoM data range. *T*CHL*a* was ~300 ng L^{-1} at the DCM in all three sites, which is 3–7-fold higher than surface values. The highest accessory pigment concentration at the DCM was for *T*CHL*b*, a pigment found in PRO and the A-EUK taxa CHLOR and PRAS*3*. Accordingly, CHLOR was often the second-most dominant A-EUK taxa (after PRYM) at our GoM sites. Taxonomically, PRAS*3* is part of CHLOR (Chlorophyceae, or green algae), but PRAS*3* is the only prasinoxanthin-containing member (Higgens *et al.*, 2011). The pigment PRAS was higher at BATS and GoM versus HOT, and the taxon PRAS*3* had a higher concentration in the GoM community when DCMs were shallower. Sequencing data have shown that prasinophytes dominate the MVCHL*b*-containing Chlorophycea in oceanic waters, suggesting that many of the CHLOR we found in the

GoM could belong to non-PRAS containing prasinophytes (dos Santos *et al.*, 2017; Rii *et al.*, 2016).

After *T*CHL*b*, the accessory pigments HEX and BUT were present at the highest concentrations at all three sites (Table VI). PRYM and PELAG, their corresponding taxa, are thus important members of the phytoplankton community. Both of these taxa are dominated by pico-sized members, as are prasinophytes (Cuvelier *et al.*, 2010; Jardillier *et al.*, 2010; Moon-van der Staay *et al.*, 2000; Raven, 2012; Worden *et al.*, 2012), suggesting that the bulk of the taxa at our GoM sites were picoplanktonic, consistent with our microscopy and FCM data.

GoM FUCO was much lower than the HOT annual mean in surface waters; however, it was similar at the DCM and within the large range of values found at BATS (Table VI). FUCO, while used as an indicator pigment for DIAT, is also present to a lesser degree in PRYM and PELAG. Since these latter two taxa had a much higher concentration at the GoM sites as evinced by HEX and BUT concentrations, the FUCO was mostly associated with these taxa. Microscopy data confirmed that DIAT were present at only very low concentrations. Given the low silicic acid associated with the Loop Current (Barbero *et al.*, 2019), it follows that DIAT were largely absent in deep GoM waters remote from land-influences. Nevertheless, DIAT, like PER, the diagnostic pigment for A-DINO, were a slightly larger proportion of the total community in the DCM relative to the ML.

Thus, with regard to PRO and SYN, our GoM stations more closely resemble BATS. However, GoM A-EUK taxonomic composition is similar to both HOT and BATS, and all are dominated by pico-phytoplankton. The oligotrophic GoM, under the influence of the Loop Current, therefore is a picoplankton-dominated system with a taxonomic composition very similar to the mean composition of BATS.

CONCLUSIONS

Phytoplankton taxa in the oceanic GoM were dominated by largely picoplanktonic PRO and PRYM throughout the euphotic zone, but the community was more diverse in the DCM, as well as having somewhat more nano- and microplankton, with CHLOR, PELAG, PRAS*3* and CRYPT, and slightly higher DIAT and A-DINO. These two spatially-separated phytoplankton communities potentially represent distinct higher trophic level pathways for primary production. Shallower DCMs (proxy for the nitracline) were correlated with more PRYM and PRAS*3* and fewer PRO. Despite some surface mixing between fresh and salt waters on the Mississippi Slope and the Florida Escarpment during the 2018 cycles (C4, C5), ML phytoplankton showed no significant change in taxonomic composition, suggesting that surface submesoscale variability was small. These trends in ML and DCM taxonomic composition likely reflect ML populations relying mainly on remineralized (ammonia) nitrogen, and the more taxonomically diverse DCM populations using some new (nitrate) nitrogen. Despite similar surface *T*CHL*a*, study sites in the central GoM (C1) and the eastern side of the basin (C5) had very different T-S properties, phytoplankton biomass profiles, and total integrated AC, illustrating the value of depth-resolved measurements. Larval ABT were found in waters with a coastal influence within ~2 weeks of sampling; suggesting that food web dynamics in these picoplankton-dominated waters are key to ABT early life survival.

SUPPLEMENTARY DATA

Supplementary data are available at the *Journal of Plankton Research* online.

DATA ARCHIVING

Data are archived for this project at the NOAA data repository at the National Centers for Coastal Ocean Science (NCCOS), and will also be archived at the Biological and Chemical Oceanography Data Management Office (BCO-DMO) site.

ACKNOWLEDGMENTS

We thank the captain and crew of the NOAA vessel *Nancy Foster* for their outstanding support at sea, as well as the overall leadership of John Lamkin, Trika Gerard and Estrella Malca for this project as a whole. We also thank Scott Ferguson of the University of Hawaii Ocean Technology Group (NF1704) and Don Cucchiara at Marine Operations of RSMAS/University of Miami (NF1802) for the use of their Biospherical Instruments PAR sensor aboard our cruises. We thank Jennifer Beatty for help at sea. Mikel Latasa and Andres Gutierrez-Rodrigues are thanked for their invaluable advice in use of the CHEMTAX program; however, Selph is fully responsible for any errors in its application to this data set. We also gratefully acknowledge advice from Rachel Foster at Stockholm University with regard to at-sea *Trichodesmium* collections. BATS pigment data is from the Bermuda Institute of Ocean Sciences (bats.bios.edu/bats-data), accessed October, 2020. HOT pigment data is from the Hawaii Ocean Time-series HOT-DOGS application at the University of Hawai'i at Mānoa (NSF Award #1756517), accessed in October, 2020. This is SOEST contribution No. 11203.

FUNDING

The National Oceanic and Atmospheric Administration (NOAA) Restore Science Program (for the project, "Effects of Nitrogen Sources

and Plankton Food-Web Dynamics on Habitat Quality for the Larvae of Atlantic Bluefin Tuna in the Gulf of Mexico"); NOAA Joint Institute for Marine and Atmospheric Research (JIMAR) Cooperative Agreement (award# NA16NMF4320058); NOAA (awards NA15OAR4320071 and NA15OAR4320071); and U.S. National Science Foundation (award OCE-1851558).

REFERENCES

Agawin, N. S. R., Duarte, C. M. and Agustí, S. (2000) Nutrient and temperature control of the contribution of picoplankton to phytoplankton biomass and production. *Limnol Oceanogr*, **45**, 591–600.

Aiken, J., Hardman-Mountford, N. J., Barlow, R. *et al.* (2008) Functional links between bioenergetics and bio-optical traits of phytoplankton taxonomic groups: an overarching hypothesis with applications for ocean colour remote sensing. *J Plankton Res*, **30**, 165–181.

Barbero, L., Pierrot, D., Wanninkhof, R. *et al.* (2019) Third Gulf of Mexico ecosystems and carbon cycle (GOMECC-3) cruise. doi: doi.org/10.25923/y6m9-fy08.

Biggs, D. C. (1992) Nutrients, plankton, and productivity in a warm-core ring in the western Gulf of Mexico. *J Geophys Res, Oceans*, **97**, 2143–2154.

Biggs, D. C. and Ressler, P. H. (2001) Distribution and abundance of phytoplankton, zooplankton, ichthyoplankton, and micronekton in the Deepwater Gulf of Mexico. *Gulf Mex Sci*, **19**, 7–29.

Bouman, H. A., Ulloa, O., Scanlan, D. J. *et al.* (2006) Oceanographic basis of the global surface distribution of *Prochlorococcus* ecotypes. *Science*, **312**, 918–921.

Brix, H., Gruber, N., Karl, D. M. and Bates, N. R. (2006) On the relationships between primary, net community, and export production in subtropical gyres. *Deep-Sea Res II Top Stud Oceanogr*, **53**, 698–717.

Brown, S. L., Landry, M. R., Selph, K. E. *et al.* (2008) Diatoms in the desert: plankton community response to a mesoscale eddy in the subtropical North Pacific. *Deep-Sea Res II Top Stud Oceanogr*, **55**, 1321–1333.

Buitenhuis, E. T., Li, W. K., Vaulot, D. *et al.* (2012) Picophytoplankton biomass distribution in the global ocean. *Earth Syst Sci Data*, **4**, 37–46.

Carpenter, E. J., Subramaniam, A. and Capone, D. G. (2004) Biomass and primary productivity of the cyanobacterium *Trichodesmium* spp. in the tropical N Atlantic Ocean. *Deep Sea Res I*, **51**, 173–203.

Chakraborty, S. and Lohrenz, S. E. (2015) Phytoplankton community structure in the river-influenced continental margin of the northern Gulf of Mexico. *Mar Ecol Prog Ser*, **521**, 31–47.

Claustre, H., Bricaud, A., Babin, M. *et al.* (2002) Diel variations in *Prochlorococcus* optical properties. *Limnol Oceanogr*, **47**, 1637–1647.

Cullen, J. J. and Eppley, R. W. (1981) Chlorophyll maximum layers of the Southern California bight and possible mechanisms of their formation and maintenance. *Oceanolog Act*, **4**, 23–32.

Cuvelier, M. L., Allen, A. E., Monier, A. *et al.* (2010) Targeted metagenomics and ecology of globally important uncultured eukaryotic phytoplankton. *Proc Natl Acad Sci U S A*, **107**, 14679–14684.

Domingues, R., Goni, G., Bringas, F. *et al.* (2016) Variability of preferred environmental conditions for Atlantic bluefin tuna (*Thunnus thynnus*) larvae in the Gulf of Mexico during 1993–2011. *Fish Oceanogr*, **25**, 320–336.

DOS Santos, A. L., Gourvil, P., Tragin, M. *et al.* (2017) Diversity and oceanic distribution of prasinophytes clade VII, the dominant group of green algae in oceanic waters. *ISME J*, **11**, 512–528.

DuRand, M. D., Olson, R. J. and Chisholm, S. W. (2001) Phytoplankton population dynamics at the Bermuda Atlantic time-series station in the Sargasso Sea. *Deep-Sea Res II Top Stud Oceanogr*, **48**, 1983–2003.

Easson, C. G. and Lopez, J. V. (2019) Depth-dependent environmental drivers of microbial plankton community structure in the northern Gulf of Mexico. *Front Microbiol*, **9**, 3175.

Elliott, B. A. (1982) Anticyclonic rings in the Gulf of Mexico. *J Phys Oceanogr*, **12**, 1292–1309.

Eppley, R. W., Carlucci, A. F., Holm-Hansen, O. *et al.* (1971) Phytoplankton growth and composition in shipboard cultures supplied with nitrate, ammonium, or urea as the nitrogen source. *Limnol Oceanogr*, **16**, 741–751.

Finkel, Z. V., Beardall, J., Flynn, K. J. *et al.* (2010) Phytoplankton in a changing world: cell size and elemental stoichiometry. *J Plankton Res*, **32**, 119–137.

Flombaum, P., Wang, W., Primeau, F. W. and Martiny, A. C. (2020) Global picophytoplankton niche partitioning predicts overall positive response to ocean warming. *Nat Geosci*, **13**, 116–120.

Friedrichs, M. A., Carr, M. E., Barber, R. T. *et al.* (2009) Assessing the uncertainties of model estimates of primary productivity in the tropical Pacific Ocean. *J Mar Syst*, **76**, 113–133.

Garrison, D. L., Gowing, M. M., Hughes, M. P. *et al.* (2000) Microbial food web structure in the Arabian Sea: a US JGOFS study. *Deep-Sea Res II Top Stud Oceanogr*, **47**, 1387–1422.

Geider, R. J. (1987) Light and temperature dependence of the carbon to chlorophyll a ratio in microalgae and cyanobacteria: implications for physiology and growth of phytoplankton. *New Phytol*, 1–34.

Gerard, T., Lamkin, R. T., Kelly, T. B. *et al.* (2021) Bluefin larvae in Oligotrophic Ocean Foodwebs, investigations of nutrients to zooplankton: overview of the BLOOFINZ-Gulf of Mexico study. *J Plankton Res*.

Goericke, R. (1998) Response of phytoplankton community structure and taxon-specific growth rates to seasonally varying physical forcing in the Sargasso Sea off Bermuda. *Limnol Oceanogr*, **43**, 921–935.

Gomez, F. A., Lee, S., Liu, Y. *et al.* (2018) Seasonal patterns in phytoplankton biomass across the northern and deep Gulf of Mexico: a numerical model study. *Biogeosci*, **15**, 3567–3576.

Hidalgo-González, R. M. and Alvarez-Borrego, S. (2008) Water column structure and phytoplankton biomass profiles in the Gulf of Mexico. *Cienc Mar*, **34**, 197–212.

Hidalgo-González, R. M., Alvarez-Borrego, S., Fuentes-Yaco, C. and Platt, T. (2005) Satellite-derived total and new phytoplankton production in the Gulf of Mexico. *Indian J Mar Sci*, **34**, 408–417.

Higgens, H., Wright, S. and Schlüter, L. (2011) Quantitative interpretation of chemotaxonomic pigment data. In Roy, S., Llewellyn, C., Egeland, E. and Johnsen, G. (eds.), *Phytoplankton Pigments: Characterization*, Cambridge University Press, Cambridge, Chemotaxonomy and Applications in Oceanography, pp. 257–313.

Holl, C. M., Villareal, T. A., Payne, C. D. *et al.* (2007) *Trichodesmium* in the western Gulf of Mexico: $^{15}N_2$-fixation and natural abundance stable isotopic evidence. *Limnol Oceanogr*, **52**, 2249–2259.

Hooker, S. B., Clementson, L., Thomas, C. S. *et al.* (2012) The fifth SeaWiFS HPLC analysis round-robin experiment (SeaHARRE-5). NASA/TM-2012-217503, NASA greenbelt, MD. 98.

Jardillier, L., Zubkov, M. V., Pearman, J. and Scanlan, D. J. (2010) Significant CO_2 fixation by small prymnesiophytes in the subtropical and tropical Northeast Atlantic Ocean. *ISME J*, **4**, 1180–1192.

Jochem, F. J. (2003) Photo- and heterotrophic pico- and nanoplankton in the Mississippi River plume: distribution and grazing activity. *J Plankton Res*, **25**, 1201–1214.

Jochens, A. E. and DiMarco, S. F. (2008) Physical oceanographic conditions in the Deepwater Gulf of Mexico in summer 2000-2002. *Deep-Sea Res II Top Stud Oceanogr*, **55**, 2541–2554.

Kelly, T. B., Knapp, A. N., Landry, M. R., Selph, K. E., Shropshire, T. A., Thomas, R. and Stukel, M. R. (2021) Lateral advection supports nitrogen export in the oligotrophic open-ocean Gulf of Mexico. *Nat Commun*.

Knapp, A. N., Thomas, R., Stukel, M. R. *et al.* (2021) Constraining the sources of nitrogen fueling phytoplankton and food webs in the Gulf of Mexico using nitrogen isotope budgets. *J Plankton Res*.

Krause, J. W., Lomas, M. W. and Nelson, D. M. (2009) Biogenic silica at the Bermuda Atlantic time-series study site in the Sargasso Sea: temporal changes and their inferred controls based on a 15-year record. *Global Biogeochem Cycles*, **23**. doi: doi.org/10.1029/2008GB003236.

Landry, M. R., Ohman, M. D., Goericke, R. *et al.* (2009) Lagrangian studies of phytoplankton growth and grazing relationships in a coastal upwelling ecosystem off Southern California. *Prog Oceanogr*, **83**, 208–216.

Landry, M. R., Selph, K. E., Stukel, M. R. *et al.* (2021) Microbial food web dynamics in the oceanic Gulf of Mexico. *J Plankton Res*.

Landry, M. R. and Swalethorp, R. (2021) Mesozooplankton biomass, grazing and trophic structure in the bluefin tuna spawning area of the oceanic Gulf of Mexico. *J Plankton Res*.

Latasa M, Gutiérrez-Rodríguez A, Cabello AMM, Scharek R. Influence of light and nutrients on the vertical distribution of marine phytoplankton groups in the deep chlorophyll maximum. *Sci Mar* 2016;**80**(S1):57–62.

Latasa, M., Scharek, R., Vidal, M. *et al.* (2010) Preferences of phytoplankton groups for waters of different trophic status in the northwestern Mediterranean Sea. *Mar Ecol Prog Ser*, **407**, 27–42.

Leipper, D. F. (1970) A sequence of current patterns in the Gulf of Mexico. *J Geophys Res*, **75**, 637–657.

Lenes, J. M., Prospero, J. M., Landing, W. M. *et al.* (2012) A model of Saharan dust deposition to the eastern Gulf of Mexico. *Mar Chem*, **134**, 1–9.

Letelier, R. M., Bidigare, R. R., Hebel, D. V. *et al.* (1993) Temporal variability of phytoplankton community structure based on pigment analysis. *Limnol Oceanogr*, **38**, 1420–1437.

Li, W. K. W., Zohary, T., Yacobi, Y. Z. and Wood, A. M. (1993) Ultraphytoplankton in the eastern Mediterranean Sea: towards deriving phytoplankton biomass from flow cytometric measurements of abundance, fluorescence and light scatter. *Mar Ecol Prog Ser*, **102**, 79–87.

Lindo-Atichati, D., Bringas, F., Goni, G. *et al.* (2012) Varying mesoscale structures influence larval fish distribution in the northern Gulf of Mexico. *Mar Ecol Prog Ser*, **463**, 245–257.

Liu, H., Dagg, M., Campbell, L. and Urban-Rich, J. (2004) Picophytoplankton and bacterioplankton in the Mississippi River plume and its adjacent waters. *Estuar*, **27**, 147–156.

Liu, H., Nolla, H. A. and Campbell, L. (1997) *Prochlorococcus* growth rate and contribution to primary production in the equatorial and subtropical North Pacific Ocean. *Aquat Microb Ecol*, **12**, 39–47.

Love, M., Baldera, A., Yeung, C. and Robbins, C. (2013) *The Gulf of Mexico Ecosystem: A Coastal and Marine Atlas*, Ocean Conservancy, Gulf Restoration Center, New Orleans, LA.

Malmstrom, R. R., Coe, A., Kettler, G. C., Martiny, A. C., Frias-Lopez, J., Zinser, E. R. and Chisholm, S. W. (2010) Temporal dynamics of Prochlorococcus ecotypes in the Atlantic and Pacific oceans. *ISME J.*, **4**, 1252–1264.

Mann, E. L. and Chisholm, S. W. (2000) Iron limits the cell division rate of *Prochlorococcus* in the eastern equatorial Pacific. *Limnol Oceanogr*, **45**, 1067–1076.

Marañón, E. (2019) Phytoplankton size structure. *Encyclopedia of Ocean Sciences (Third Ed)*, **1**, 599–605.

Marra, J. F., Lance, V. P., Vaillancourt, R. D. and Hargreaves, B. R. (2014) Resolving the ocean's euphotic zone. *Deep Sea Res I*, **83**, 45–50.

Martínez-López, B. and Zavala-Hidalgo, J. (2009) Seasonal and interannual variability of cross-shelf transports of chlorophyll in the Gulf of Mexico. *J Mar Syst*, **77**, 1–20.

Menden-Deuer, S. and Lessard, E. J. (2000) Carbon to volume relationships for dinoflagellates, diatoms, and other protist plankton. *Limnol Oceanogr*, **45**, 569–579.

Michaels, A. F. and Silver, M. W. (1988) Primary production, sinking fluxes and the microbial food web. *Deep-Sea Res*, **35**, 473–490.

Monger, B. C. and Landry, M. R. (1993) Flow cytometric analysis of marine bacteria with Hoechst 33342. *Appl Environ Microbiol*, **59**, 905–911.

Moon-van der Staay, S. Y., VAN DER Staay, G. W., Guillou, L. *et al.* (2000) Abundance and diversity of prymnesiophytes in the picoplankton community from the equatorial Pacific Ocean inferred from 18S rDNA sequences. *Limnol Oceanogr*, **45**, 98–109.

Morgan, K. C. and Kalff, J. (1979) Effect of light and temperature interactions on growth of *Cryptomonas erosa* (Cryptophyceae). *J Phycol*, **15**, 127–134.

Morrison, J. M. and Nowlin, W. D. (1977) Repeated nutrient, oxygen, and density sections through the loop current. *J Mar Res*, **35**, 105–128.

Mouw, C. B., Barnett, A., McKinley, G. A. *et al.* (2016) Phytoplankton size impact on export flux in the global ocean. *Global Biogeochem Cycles*, **30**, 1542–1562.

Muhling, B. A., Smith, R. H., Vasquez, L. *et al.* (2013) Larval fish assemblages and mesoscale oceanographic structure along the Mesoamerican barrier reef system. *Fish Oceanogr*, **22**, 409–428.

Mulholland, M. R., Bernhardt, P. W., Heil, C. A. *et al.* (2006) Nitrogen fixation and release of fixed nitrogen by *Trichodesmium* spp. in the Gulf of Mexico. *Limnol Oceanogr*, **51**, 1762–1776.

Müller-Karger, F. E., Smith, J. P., Werner, S. *et al.* (2015) Natural variability of surface oceanographic conditions in the offshore Gulf of Mexico. *Prog Oceanogr*, **134**, 54–76.

Müller-Karger, F. E., Walsh, J. J., Evans, R. H. and Meyers, M. B. (1991) On the seasonals phytoplankton concentration and sea surface temperature cycles of the Gulf of Mexico as determined by satellites. *J Geophys Res, Oceans*, **96**, 12645–12665.

Partensky, F., Blanchot, J., Lantoine, F. *et al.* (1996) Vertical structure of picophytoplankton at different trophic sites of the tropical northeastern Atlantic Ocean. *Deep Sea Res I*, **43**, 1191–1213.

Pasulka, A. L., Landry, M. R., Taniguchi, D. A. *et al.* (2013) Temporal dynamics of phytoplankton and heterotrophic protists at station ALOHA. *Deep-Sea Res II Top Stud Oceanogr*, **93**, 44–57.

Qian, Y., Jochens, A. E., Kennicutt, M. C. II and Biggs, D. C. (2003) Spatial and temporal variability of phytoplankton biomass and community structure over the continental margin of the Northeast Gulf of Mexico based on pigment analysis. *Cont Shelf Res*, **23**, 1–17.

Raven, J. A. (2012) Algal biogeography: metagenomics shows distribution of a picoplanktonic pelagophyte. *Curr Biol*, **22**, R682–R683.

Richardson, K. and Bendtsen, J. (2019) Vertical distribution of phytoplankton and primary production in relation to nutricline depth in the open ocean. *Mar Ecol Prog Ser*, **620**, 33–46.

Riemann, B., Simonsen, P. and Stensgaard, L. (1989) The carbon and chlorophyll content of phytoplankton from various nutrient regimes. *J Plankton Res*, **11**, 1037–1045.

Rii, Y. M., Duhamel, S., Bidigare, R. R. *et al.* (2016) Diversity and productivity of photosynthetic picoeukaryotes in biogeochemically distinct regions of the south East Pacific Ocean. *Limnol Oceanogr*, **61**, 806–824.

Roman, M. R., Adolf, H. A., Landry, M. R. *et al.* (2001) Estimates of oceanic mesozooplankton production: a comparison using the Bermuda and Hawaii time-series data. *Deep-Sea Res II Top Stud Oceanogr*, **49**, 175–192.

Ryther, J. H. (1956) Photosynthesis in the ocean as a function of light intensity. *Limnol Oceanogr*, **1**, 61–70.

Saba, V. S., Friedrichs, M., Carr, M.-E. *et al.* (2010) Challenges of modeling depth-integrated marine primary productivity over multiple decades: a case study at BATS and HOT. *Global Biogeochem Cycles*, **24**. doi: doi/abs/10.1029/2009GB003655.

Salas-de-León, D. A., Monreal-Gómez, M. A., Signoret, M. and Aldeco, J. (2004) Anticyclonic-cyclonic eddies and their impact on near-surface chlorophyll stocks and oxygen supersaturation over the Campeche canyon, Gulf of Mexico. *J Geophys Res, Oceans*, **109**, 1–10.

Sansón, L. Z. and Provenzale, A. (2009) The effects of abrupt topography on plankton dynamics. *Theo Pop Biol*, **76**, 258–267.

Selph, K. E., Landry, M. R., Taylor, A. G. *et al.* (2011) Spatially-resolved taxon-specific phytoplankton production and grazing dynamics in relation to iron distributions in the equatorial Pacific between 110 and 140°W. *Deep-Sea Res II*, **58**, 358–377.

Shalapyonok, A., Olson, R. J. and Shalapyonok, L. S. (2001) Arabian Sea phytoplankton during southwest and northeast monsoons 1995: composition, size structure and biomass from individual cell properties measured by flow cytometry. *Deep-Sea Res II Top Stud Oceanogr*, **48**, 1231–1261.

Sherr, B. F. and Sherr, E. B. (1993) Preservation and storage of samples for enumeration of heterotrophic protists. In Sherr, B. F., Sherr, E. B. and Cole, J. J. (eds.), *Kemp, P. F*, CRC Press, Handbook of Methods in Aquatic Microbial Ecology, pp. 207–212.

Steinberg, D. K., Carlson, C. A., Bates, N. R. *et al.* (2001) Overview of the US JGOFS Bermuda Atlantic time-series study (BATS): a decade-scale look at ocean biology and biogeochemistry. *Deep-Sea Res II Top Stud Oceanogr*, **48**, 1405–1447.

Strickland, J. D. H. and Parsons, T. R. (1972) A practical handbook of seawater analysis. *Bull Fish Res Board Can*, **167**, 1–130.

Stukel, M. R., Gerard, T., Kelly, T. B., Knapp, A. N., Laiz-Carrión, R., Lamkin, J. T., Landry, M. R., *et al.* (2021a) Plankton food webs in the oligotrophic Gulf of Mexico spawning grounds of Atlantic Bluefin tuna. *J Plankton Res*

Stukel, M. R., Kelly, T. B., Landry, M. R. *et al.* (2021b) Sinking carbon, nitrogen, and pigment flux within and beneath the euphotic zone in the oligotrophic, open-ocean Gulf of Mexico. *J Plankton Res*.

Taylor, A. G., Landry, M. R., Selph, K. E. and Wokuluk, J. J. (2015) Temporal and spatial patterns of microbial community biomass and composition in the Southern California current ecosystem. *Deep-Sea Res II Top Stud Oceanogr*, **112**, 117–128.

Taylor, A. G., Landry, M. R., Selph, K. E. and Yang, E. J. (2011) Biomass, size structure and depth distributions of the microbial community in the eastern equatorial Pacific. *Deep-Sea Res II*, **58**, 342–357.

Teo, S. L., Boustany, A., Dewar, H. *et al.* (2007) Annual migrations, diving behavior, and thermal biology of Atlantic bluefin tuna, *Thunnus thynnus*, on their Gulf of Mexico breeding grounds. *Mar Biol*, **151**, 1–18.

Uitz J, Claustre H, Gentili B, Stramski D. Phytoplankton class-specific primary production in the world's oceans: seasonal and interannual variability from satellite observations. *Global Biogeochem Cycles* 2010;**24**(3). doi: doi/full/10.1029/2009GB003680.

Van Heukelem, L. and Thomas, C. S. (2001) Computer-assisted high-performance liquid chromatography method development with applications to the isolation and analysis of phytoplankton pigments. *J Chromatogr A*, **910**, 31–49.

Vaulot, D., Marie, D., Olson, R. J. and Chisholm, S. W. (1995) Growth of *Prochlorococcus*, a photosynthetic prokaryote, in the equatorial Pacific Ocean. *Science*, **268**, 1480–1482.

Veldhuis, M. J. and Kraay, G. W. (2004) Phytoplankton in the subtropical Atlantic Ocean: towards a better assessment of biomass and composition. *Deep Sea Res I*, **51**, 507–530.

Vukovich, F. M. (2007) Climatology of ocean features in the Gulf of Mexico using satellite remote sensing data. *J Phys Oceanogr*, **37**, 689–707.

Walsh, J. J. and Steidinger, K. A. (2001) Saharan dust and Florida red tides: the cyanophyte connection. *J Geophys Res, Oceans*, **106**, 11597–11612.

Wang, L., Huang, B., Laws, E. A. *et al.* (2018) Anticyclonic eddy edge effects on phytoplankton communities and particle export in the northern South China Sea. *J Geophys Res, Oceans*, **123**, 7632–7650.

Wawrik, B. and Paul, J. H. (2004) Phytoplankton community structure and productivity along the axis of the Mississippi River plume in oligotrophic Gulf of Mexico waters. *Aquat Microb Ecol*, **35**, 185–196.

Westberry T, Behrenfeld MJ, Siegel DA, Boss E. Carbon-based primary productivity modeling with vertically resolved photoacclimation. *Global Biogeochem Cycles* 2008;**22**(2). doi: doi/full/10.1029/2007GB003078.

Williams, A. K., McInnes, A. S., Rooker, J. R. and Quigg, A. (2015) Changes in microbial plankton assemblages induced by mesoscale oceanographic features in the northern Gulf of Mexico. *PLoS One*, **10**, e0138230.

Worden, A. Z., Janouskovec, J., McRose, D. *et al.* (2012) Global distribution of a wild alga revealed by targeted metagenomics. *Curr Biol*, **22**, R675–R677.

Worden, A. Z., Nolan, J. K. and Palenik, B. (2004) Assessing the dynamics and ecology of marine picophytoplankton: the importance of the eukaryotic component. *Limnol Oceanogr*, **49**, 168–179.

Wright, S. (2008) Chemtax version 1.95 for calculating the taxonomic composition of phytoplankton populations, Ver. 1, Australian Antarctic data Centre. doi: 10.4225/15/59fff1c5ea8fc Accessed: 2020-06-01.

Yingling, N., Kelly, T. B., Shropshire, T. A. *et al.* (2021) Taxon-specific phytoplankton growth, nutrient utilization, and light limitation in the oligotrophic Gulf of Mexico. *J Plankton Res*.

Zettler, E. R., Olson, R. J., Binder, B. J. *et al.* (1996) Iron-enrichment bottle experiments in the equatorial Pacific: responses of individual phytoplankton cells. *Deep-Sea Res II Top Stud Oceanogr*, **43**, 1017–1029.